Bandwidth Analysis of Multiport Radio-Frequency Systems—Part II

Ding Nie, *Student Member, IEEE,* and Bertrand M. Hochwald, *Fellow, IEEE*

***Abstract*—We analyze the bandwidth over which power can be transferred from multiple radio-frequency sources to multiple loads through a passive multiport matching network. This is the second part of a two-part paper. In the first part we introduce broadband multiport matching upper bounds and apply them to determine the bandwidth of loads and network structures whose scattering parameters can be expressed analytically with rational functions. In this second part, we apply the bounds to loads, such as antennas, whose scattering parameters are obtained by measurement or simulation. We focus on the effects of coupling on bandwidth. Since the bounds require frequency responses that are rational functions, we provide guidelines on how to obtain rational approximations for arbitrary loads. Complete derivations of the bounds are also provided.**

***Index Terms*—Bandwidth, Bode-Fano bounds, broadband matching bounds, non-reciprocal networks, passive matching networks, radio-frequency coupling**

I. Introduction

We analyze the bandwidth over which power can be transferred from M sources through a passive matching network to N loads in radio-frequency (RF) systems. Our principal tools include broadband matching upper bounds, which are presented in Part I of this paper [1], and briefly repeated herein for easy reference. These bounds extend the classical Bode-Fano results [2], [3], which apply to a single source and load. The bounds depend only on the scattering matrix (S-matrix) of the loads. The loads may be electromagnetically coupled to each other.

In this part, we apply the bounds to loads whose S-matrix is expressed numerically, found through either measurements or simulations. The bounds require rational models of the loads that can be obtained through fitting of the numerical data. We provide guidelines for assessing the accuracy of a rational model.

Of particular interest is the effect of coupling on the bandwidth of multiple antennas. One example demonstrates that the bandwidth bound of a pair of dipoles fluctuates non-monotonically with the distance between them, and, with the right amount of coupling, can be significantly greater than for decoupled dipoles. We focus on the "input bandwidth" of the loads, and are not concerned with how efficiently the loads use their input power.

We also include complete derivations of the bounds. These derivations are not needed to apply the bounds but are of use in understanding how the conditions for equality in the bound apply.

The notations and definitions are identical to those in Part I. We assume M decoupled sources with characteristic impedance Z_0 drive N loads that have a frequency-dependent $N \times N$ S-matrix $S_L(s)$, where $s = \sigma + j\omega$ is the extension of frequency $j\omega$ to the whole complex plane (WCP). An $(M+N)$-port passive matching network is inserted between the sources and loads. Our measure of the quality of matching is the power loss ratio $r^2(\omega) \in [0,1]$, defined as the ratio between the total power lost, including insertion and return losses, and the total incident power from the sources at frequency ω. The insertion loss is the power dissipated in the matching network; the return loss is the power reflected to the sources. Since the loads are potentially coupled, the quantity $r^2(\omega)$ captures the possibility that incident power from one source can reflect back to itself or to other sources. We then define the bandwidth $\omega_{\text{BW}}(\tau, \omega_d)$ as the frequency range for which $r(\omega)$ (the positive square root of $r^2(\omega)$) is no greater than a threshold $\tau > 0$ in the vicinity of a design frequency ω_d. The mathematical definitions of $r(\omega)$ and $\omega_{\text{BW}}(\tau, \omega_d)$ can be found in Part I.

We generally employ the properties of S-matrices of passive real networks to prove the bounds; these properties include real-rational, Hurwitzian and bounded. We also use the definitions of poles and zeros of rational matrices. We use LHP to denote the left-half complex plane ($\text{Re}\{s\} < 0$) and RHP to denote the right-half ($\text{Re}\{s\} > 0$).

A. Summary of bounds

There are three bounds which are summarized as follows. If

$$S_L^T(-s_0)S_L(s_0) = I \tag{1}$$

is satisfied for some $\text{Re}\{s_0\} \geq 0$, then the following inequality holds for any passive matching network:

$$\int_0^\infty f(\omega) \log \frac{1}{r(\omega)} d\omega \leq B, \tag{2}$$

where $f(\omega)$ and B depend on the location of s_0 and are given in Table I. To compute the bound B, the poles and zeros of $S_L(s)$, denoted as $p_{L,i}, z_{L,i}$, are also needed. We refer to rows 1, 2, and 3 in Table I as Bounds 1, 2, and 3.

The bounds depend on the poles and zeros of the real-rational matrix $S_L(s)$, which we explain how to obtain in Section II. We focus on the steps needed to fit realistic loads with rational models. Bandwidth analyses of various loads are

Ding Nie and Bertrand Hochwald are with the Department of Electrical Engineering, University of Notre Dame, Notre Dame, IN, 46556 USA. E-mail: nding1@nd.edu, bhochwald@nd.edu.

This work was supported, in part, by NSF grants CCF-1403458 and ECCS-1509188.

TABLE I
FORMS OF $f(j\omega)$ AND B IN (2) FOR DIFFERENT LOCATIONS OF s_0, WHERE $p_{L,i}, z_{L,i}$ ARE THE POLES AND ZEROS OF $S_L(s)$.

$s_0 = j\omega_0$	$f(\omega) = \frac{1}{2}[(\omega_0 - \omega)^{-2} + (\omega_0 + \omega)^{-2}]$ $B = \frac{-\pi}{2M}\left[\sum_i (p_{L,i} - j\omega_0)^{-1} + \sum_i (z_{L,i} + j\omega_0)^{-1}\right]$
$\mathrm{Re}\{s_0\} > 0$	$f(\omega) = \frac{1}{2}\mathrm{Re}[(s_0 - j\omega)^{-1} + (s_0 + j\omega)^{-1}]$ $B = \frac{-\pi}{2M}\log\left\lvert\det S_L(s_0)\cdot\frac{\prod_i (s_0+z_{L,i})}{\prod_i (s_0-z_{L,i})}\right\rvert$
$s_0 = \infty$	$f(\omega) = 1$ $B = \frac{-\pi}{2M}\left(\sum_i p_{L,i} + \sum_i z_{L,i}\right)$

then presented in Section III. The bounds are corollaries of Theorems 2 and 3, which are presented in Section IV. We conclude in Section V.

II. OBTAINING $S_L(s)$ AND ITS POLES AND ZEROS

The matrix $S_L(s) = (Z_L(s) + Z_0 I)^{-1}(Z_L(s) - Z_0 I)$ is uniquely determined if the impedance matrix of the loads $Z_L(s)$ is known analytically. For many realistic loads, this is generally impossible. Instead, either $Z_L(j\omega)$ or $S_L(j\omega)$ is often obtained as the result of a numerical simulation or measurement, where ω is contained to some frequency range of interest. The next section gives an example of how to use the results of simulation to find $S_L(s)$.

A. Finding $S_L(s)$ from numerical simulations of loads

The following steps can be used to find $S_L(s)$:

a) Measure or simulate the loads in the frequency range of interest $[\omega_1, \omega_2]$. Denote the measured response $S'_L(j\omega)$.
b) Find a passive rational $S_L(s)$ such that $S_L(j\omega)$ is "close enough" to $S'_L(j\omega)$ for $\omega \in [\omega_1, \omega_2]$.

Step a) can be done with standard modeling software such as Ansys HFSS in the case of simulations, or a network analyzer in the case of measurements. Step b) can be accomplished by fitting rational functions to the individual entries of $S'_L(j\omega)$ using, for instance, the Matrix Fitting Toolbox [4]–[8] in MATLAB. We have more to say about this fitting in the next section.

To compute the right-hand side of (2):

c) Find an s_0 where (1) is satisfied for the computed $S_L(s)$.
d) Calculate the poles and zeros $p_{L,i}, z_{L,i}$ of $S_L(s)$.

Step c) requires us to solve $S_L^T(-s_0)S_L(s_0) = I$. For $s_0 = j\omega_0$, we can instead solve $|\det S_L(j\omega_0)| = 1$. For Step d), $p_{L,i}, z_{L,i}$ can be obtained from the definitions of poles and zeros of matrices. In some cases the poles and zeros of $S_L(s)$ coincide with the poles and zeros of $\det S_L(s)$. One way of checking this is presented in [9], which we do not repeat here. Then $p_{L,i}, z_{L,i}$ can be obtained by applying root-finding algorithms to $1/\det S_L(s) = 0$ and $\det S_L(s) = 0$, respectively. The examples shown in Sections III-B–III-E use this approach.

Multiple rational models may exist within the error tolerance of $S'_L(j\omega)$ for $\omega \in [\omega_1, \omega_2]$. Each model could satisfy (1) for different s_0, and generate different bounds. When these models yield consistent results, one can build confidence that the bounds and models are physically meaningful. When these models contradict each other, further investigation is needed to determine the source of the inconsistency. An example of multiple models is shown in Section III-C.

B. Analysis of distributed-element loads using rational models

Since $S_L(s)$ is a real-rational matrix, accurate modeling of lumped-circuit loads is straightforward and can be done without error. However, many loads such as antennas, transmission lines, and other distributed-element systems include time-delays, stubs, and other structures that are often modeled using non-rational functions of s. A real-rational $S_L(s)$ is then needed that "approximates" the loads with sufficient accuracy to obtain a meaningful bandwidth bound.

The numerical and analytical approximation of distributed-element circuits by lumped circuits over a fixed bandwidth is a topic that has been studied in many contexts. An early example is [10]. A summary of some practical techniques can be found in [11]. Recent advances in antenna modeling include [12]. Other fields such as control engineering use rational fitting extensively [13].

The mathematical problem of rational approximation and modeling is addressed by Runge's theorem in complex analysis [14], which states that any analytical function on a subset of the complex plane can be fit arbitrarily precisely with rational functions. For example, the Padé approximation [15], [16] is often used to model time delays using rational functions over a frequency band of interest.

We are interested in obtaining an upper bound on

$$\int_{\omega_1}^{\omega_2} f(\omega)\log\frac{1}{r'(\omega)}d\omega, \tag{3}$$

where $r'(\omega)$ is the loss experienced when the matching network is used with the actual loads $S'_L(j\omega)$. The process outlined in Section II-A creates a rational approximation $S_L(j\omega)$ for $\omega \in [\omega_1, \omega_2]$. For an arbitrary matching network, (2) gives

$$\int_{\omega_1}^{\omega_2} f(\omega)\log\frac{1}{r(\omega)}d\omega \le \int_0^{\infty} f(\omega)\log\frac{1}{r(\omega)}d\omega \le B, \tag{4}$$

where B is computed from $S_L(s)$ and $r(\omega)$ is the power loss ratio experienced with the loads $S_L(s)$. The difference between the left-hand sides of (3) and (4) is

$$\int_{\omega_1}^{\omega_2} f(\omega)\log\frac{r(\omega)}{r'(\omega)}d\omega,$$

and represents the error in the integral introduced by the approximation of $S'_L(j\omega)$. Then choosing $S_L(s)$ such that

$$\int_{\omega_1}^{\omega_2} f(\omega)\log\frac{r(\omega)}{r'(\omega)}d\omega \le \delta B \tag{5}$$

for some desired tolerance $\delta B > 0$ yields the bound

$$\int_{\omega_1}^{\omega_2} f(\omega)\log\frac{1}{r'(\omega)}d\omega \le B + \delta B. \tag{6}$$

The following theorem provides a first-order approximation of δB for $S_L(s)$ that is close to $S'_L(j\omega)$ in the frequency band of interest.

Theorem 1: Let $\delta S_L(j\omega) = S_L(j\omega) - S'_L(j\omega)$ and define

$$\rho(\omega) = \frac{2\sigma_{\delta,\max}(\omega)}{1-\sigma'^2_{L,\max}(\omega)} \cdot \sqrt{1 + \frac{\sigma'^2_{L,\max}(\omega) - \sigma'^2_{L,\min}(\omega)}{(1-\sigma'_{L,\max}(\omega))^2}}, \quad (7)$$

where $\sigma_{\delta,\max}(\omega)$ is the maximum singular value of $\delta S_L(j\omega)$, and $0 \le \sigma'_{L,\min}(\omega) < \sigma'_{L,\max}(\omega) < 1$ are the minimum and the maximum singular values of $S'_L(j\omega)$, respectively. Then

$$\delta B \to \int_{\omega_1}^{\omega_2} \frac{f(\omega)}{2} \log\left(1 + \frac{1-r'^2(\omega)}{r'^2(\omega)} \cdot \rho(\omega)\right) d\omega \quad (8)$$

as $\|\delta S_L(j\omega)\|_F \to 0$ for $\omega \in [\omega_1, \omega_2]$.

Proof: See Appendix A. ■

In (8), $f(\omega)$ is given in Table I, and $\rho(\omega)$ is determined by $S'_L(j\omega)$ and $\delta S_L(j\omega)$. The notation $\|\cdot\|_F$ refers to the Frobenius norm (sum of squared magnitude of entries) of a matrix. In the limit of a perfect model when $\delta S_L(j\omega) = 0$, then $\rho(\omega) = 0$ and $\delta B = 0$. In general, δB depends on $r'(\omega)$, which depends on the matching network. To eliminate the dependence of δB on $r'(\omega)$, we choose the desired goal of $r'(\omega) \approx \tau$ for $\omega \in [\omega_1, \omega_2]$, whence

$$\delta B \approx \int_{\omega_1}^{\omega_2} \frac{f(\omega)}{2} \log\left(1 + \frac{1-\tau^2}{\tau^2} \cdot \rho(\omega).\right) d\omega. \quad (9)$$

Note that even if $r'(\omega)$ does not achieve τ for $\omega \in [\omega_1, \omega_2]$, (9) is still a useful quantity because it upper-bounds δB.

The steps for evaluating goodness-of-fit are then:

e) Compute δB in (9) numerically.

f) Evaluate if the desired tolerance on $\delta B/B$ is met.

If the desired tolerance is not met, a smaller $\delta S_L(j\omega)$ is needed. Finally,

g) Compute the bound (6).

Theorem 1 can also be used to examine cases where the rational fit may fail to generate an accurate bound. For example, if $\sigma'_{L,\max}(\omega) \approx 1$ in the neighborhood of some ω, meaning $S'_L(j\omega)$ is very reflective, (7) indicates that $\rho(\omega)$ becomes large. Any attempt to make $r'(\omega)$ small around this ω could then potentially make δB in (8) large. Thus, attempting to match a load where it is naturally very reflective may lead to a loose bound.

C. Hazard of over-fitting

In attempting to make $\delta B/B$ small, care should be taken not to "over-fit" the loads. Over-fitting or over-modeling occurs when the degrees of the polynomials in the numerator and denominator of the rational functions in $S_L(s)$ are larger than needed to obtain the desired accuracy. As the polynomial degrees are increased, the relative error $\delta B/B$ is decreased since δB is decreased. But there is also the hazard that B is made unnecessarily large because of the excessive number of poles and zeros in $S_L(s)$. As a result, (6) becomes loose and Condition 4 for achieving B cannot be satisfied. There is a tension between making the rational model accurate while still having a small number of poles and zeros.

One approach to determine if the system is over-fitted is to examine the poles and zeros of the entries of $S_L(s)$. Any poles and zeros that nearly cancel can have a small effect on δB but a large effect on B; they should be removed and $\delta B/B$ re-checked. Simpler models yield tighter bounds, and thus there is an incentive to find the minimal model that adequately captures the frequency response of the loads in the band of interest. A detailed discussion of modeling poles is found in [17]. A discussion of the sensitivity of poles and zeros to perturbations of the data is found in [18].

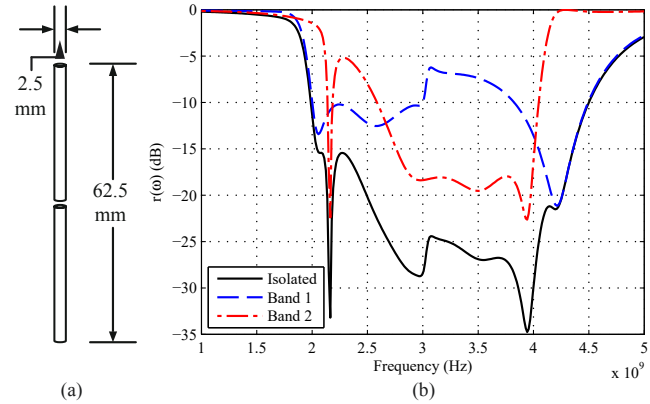

Fig. 1. (a) Geometry of a dipole that is half-wavelength at 2.4 GHz. (b) Two decoupled dipoles are matched by the structure shown in Figure 2. Matching Network 1 handles 2–3 GHz and Network 2 handles 3–4 GHz; their resulting $r(\omega)$'s are given in the blue dashed and red dash-dot curves, respectively. The overall system $r(\omega)$ is shown by the solid curve.

In the remainder, we use the notation $r(\omega)$ when we are considering the rational model, and we use $r'(\omega)$ when we are considering the actual loads. In Section III-D, we present an example where time delay in a circuit is modeled using rational functions. Section III-E computes (6) for four realistic coupled antennas.

III. Bandwidth Analysis of Antennas

We now calculate broadband matching bounds for five examples, all involving amplifiers driving antennas. Aspects of coupling and rational approximation are emphasized. The first three examples assume that the rational models are accurate and therefore compute only (2), while the last two examples incorporate the effects of rational fitting and therefore compute (6). We begin with two identical decoupled dipoles whose rational models are taken from [9].

A. Two decoupled dipoles

We design a broadband network of the type in Figure 5(b) in Part I for two decoupled dipoles ($N = 2$) with one source ($M = 1$). From Theorem 1 in Part I, the bound for two decoupled dipoles is twice as large as for a single dipole when there is only one source. The geometry of a dipole is shown in Figure 1(a), which is half-wavelength at 2.4 GHz. In [9], the same dipole is simulated in the range 1–5 GHz, and is modeled using an S-parameter model $S_l(s)$ normalized by characteristic impedance $Z_0 = 50\ \Omega$ that satisfies $S_l(\infty) = -1$. We apply the model here, and write the S-matrix of two such dipoles as $S_L(s) = \mathrm{diag}(S_l(s), S_l(s))$.

Clearly, $S_L(\infty) = -I$, and (1) is satisfied at $s_0 = \infty$. The poles and zeros of $S_l(s)$ are listed in Table III in [9], and Bound 3, using (2), for $M = 1$ gives

$$\int_{\omega_1}^{\omega_2} \log \frac{1}{r(\omega)} d\omega \leq \int_0^{\infty} \log \frac{1}{r(\omega)} d\omega \leq 4.93 \times 10^{10}, \quad (10)$$

where $\omega_1 = 2\pi \times 10^9$ and $\omega_2 = 10\pi \times 10^9$ are the lower and upper modeling frequencies.

We are interested in matching the decoupled dipoles to one source in the 2–4 GHz range. The structure in Figure 2 is employed, where Matching Network 1 is tuned for the 2–3 GHz band and Matching Network 2 is tuned for the 3–4 GHz band and one circulator is used. These two-port networks are designed using the Real Frequency Technique [19], followed by a realization using Darlington synthesis [20]. In Figure 1(b), the dashed and dash-dot curves show $r(\omega)$ of each network when connected by itself to a dipole (typically through a balun that is not shown). The $r(\omega)$ of the entire system, including circulator, is the product of the $r(\omega)$ achieved by each, and is shown as the solid curve. We seek a power reflection ratio of $r(\omega) \leq 0.2$ (-14 dB). From the figure, we see that the bandwidth achievable is $\omega_{\text{BW}}(0.2, 3 \text{ GHz}) = 2.35$ GHz. The achieved integral is

$$\int_{\omega_1}^{\omega_2} \log \frac{1}{r(\omega)} d\omega = 4.58 \times 10^{10}. \quad (11)$$

There is only a 3.51×10^9 gap between (10) and (11), which is due entirely to shaping loss defined in Part I, Section III-C. We therefore achieve excellent performance for one source and two dipoles with this non-reciprocal network. According to Theorem 3 in Part I, since $M < N$, using a reciprocal splitter or coupler as part of the network would not perform as well.

An experimental measurement of the effectiveness of the matching network in Figure 2 would require standard S-parameter measurements by a network analyzer at the input port of the circulator. Since there is only one source, no averaging is needed over phase differences, as described in Part I, Section II-C. By the definition of $r(\omega)$, and because the network is (theoretically) lossless, small values of $r(\omega)$ in 2–4 GHz imply that the power from the source is being accepted by the antennas.

We also note that for two sources ($M = 2$), we would be able to achieve only half the bandwidth for the same -14 dB threshold. Clearly, the matching network for two sources would differ considerably from the one presented in Figure 2 and could be reciprocal. We do not design such a network here.

B. Two coupled dipoles

To illustrate the effect of coupling between two parallel dipoles, we examine their bandwidth as a function of the distance between them. We assume each dipole has the same 2.4 GHz half-wavelength structure as Figure 1(a). The center feeding points of the parallel dipoles are at the same vertical level, and the distance between them is d, as measured at any place along their lengths. For each value of d, we apply the modeling recipe for the S-matrix $S_L(j\omega)$ detailed in Section II in the range 1–5 GHz. Since we wish to compare the bounds for coupled dipoles with (10), we model their S-matrices using six poles and six zeros, and enforce $S_L(\infty) = -I$. Then the resulting model $S_L(s)$ satisfies (1) at $s_0 = \infty$ for every d, and Bound 3 can be applied to compare with (10).

We let d range from 0.03λ to 1.5λ, with step size 0.01λ, where $\lambda = 125$ mm is the wavelength at 2.4 GHz. The poles and zeros $p_{L,i}, z_{L,i}$ are computed from $S_L(s)$, and Bound 3 is computed for each d. For $M = 1$ and $M = 2$, the bounds are shown in Figure 3 by the black and blue curves. The black curve values are twice the blue curve. Horizontal dotted lines indicate the bounds for decoupled dipoles.

Figure 3 shows oscillatory behavior and suggests that cou-

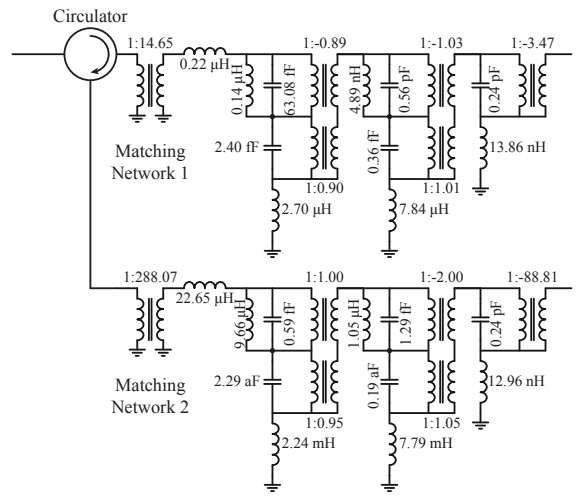

Fig. 2. Matching network of the type in Figure 5(b) in Part I is used to connect a source (on the left) to two decoupled dipoles (connected on the right, typically through baluns that are not shown). Matching networks 1 and 2 are designed using the Real Frequency Technique [19], followed by realizations using Darlington synthesis [20].

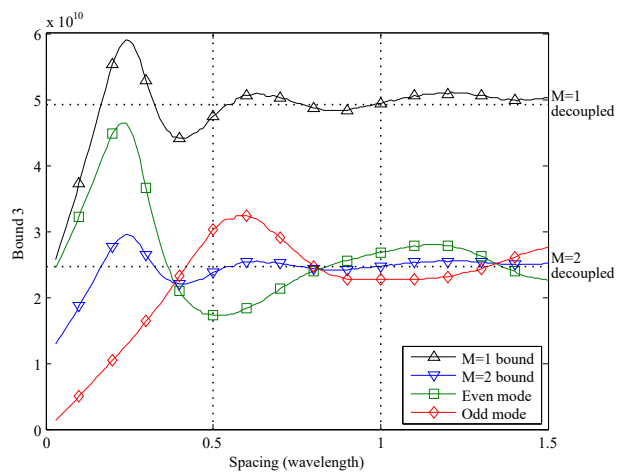

Fig. 3. Bound 3 for two parallel dipoles versus spacing d, for d between 0.03λ and 1.5λ (λ =125 mm is the wavelength at 2.4 GHz). Each dipole has the structure shown in Figure 1(a), the center feeding points of the dipoles are at the same vertical level, and the distance d is maintained along their lengths. The horizontal dotted lines indicate Bound 3 for two decoupled dipoles. Also shown are the even- and odd-mode beamforming bounds.

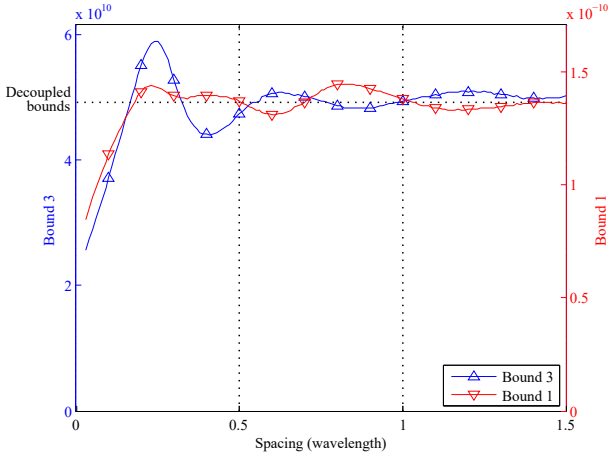

Fig. 4. For one source and two parallel dipoles with spacing d, Bound 3 (left y-axis) is compared with Bound 1 (right y-axis). Bound 3 is the same as the black curve shown in Figure 3. The dotted horizontal line indicates the limiting values for decoupled dipoles.

pled dipoles can have large bandwidths at certain distances from each other. The maxima appear near 0.24λ and are 20% larger than their decoupled-dipole counterparts. As d increases, the bounds approach the decoupled-dipole limits. On the other hand, when d approaches zero, the two dipoles merge into a single dipole, and the bounds in Figure 3 approach the bounds where M sources drive a single dipole.

We already know from Part I, Section V-A, that using these dipoles in a beamformer configuration with $M = 1$ generally cannot achieve the bound for any d. But the beamformer configuration is still worth analyzing briefly. There are two beamformers that are of special interest: even-mode and odd-mode, corresponding to $\vec{v}(s) = [1/\sqrt{2}, 1/\sqrt{2}]^T$ and $[1/\sqrt{2}, -1/\sqrt{2}]^T$ in (25) in Part I. Since the dipoles are reciprocal and have a symmetric structure, the resulting $S_L(s)$ is symmetric circulant, and both even and odd $\vec{v}(s)$ are real constant unit eigenvectors of $S_L(s)$. Thus Theorem 5 in Part I applies.

Figure 3 shows the results. Both even and odd-mode bounds are strictly smaller than the bound for $M = 1$, as expected. Their sum, however, equals the $M = 1$ bound because the incident and reflected waves to and from the loads are orthogonal for the two modes. Therefore, the modes can be treated as decoupled loads, each with its own equivalent S-parameter and bound.

C. Multiple models for the same loads

For a set of loads with a measured $S'_L(j\omega)$, more than one model $S_L(s)$ may be created within a given error tolerance. To illustrate this, we take the parallel dipoles in Section III-B with $S'_L(j\omega)$ measured in 1–5 GHz as examples. For each d, we model the S-matrix using the Matrix Fitting Toolbox with six poles and six zeros and enforce $S_L(0) = I$. The resulting $S_L(s)$ then satisfies (1) at $s_0 = 0$, and Bound 1 is applied to the coupled dipoles. We contrast the results with Section III-B, where $S_L(\infty) = -I$ is enforced and Bound 3 applies.

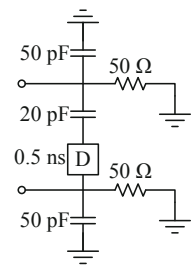

Fig. 5. Two capacitively coupled loads. The coupling includes an ideal delay component of 0.5 ns.

TABLE II
VALUES OF $p_{L,i}$ AND $z_{L,i}$ FOR $S_L(s)$ MODEL FOR THE COUPLED LOADS IN FIGURE 5. TABLE (A) SHOWS $p_{L,i}$ AND $z_{L,i}$ WHEN THE PADÉ APPROXIMATION IS APPLIED, AND TABLE (B) SHOWS $p_{L,i}$ AND $z_{L,i}$ WHEN THE LOADS ARE FITTED WITH RATIONAL MATRICES WITHOUT THE PADÉ APPROXIMATION.

(a)

i	$p_{L,i}$	$z_{L,i}$
1	-6.71×10^8	0
2, 3	$(-0.05 \pm 3.37j) \times 10^9$	$\pm 3.38j \times 10^9$
4, 5	$(-0.00 \pm 1.33j) \times 10^{10}$	$\pm 1.33j \times 10^{10}$
6	-4.35×10^8	0
7, 8	$(-0.16 \pm 1.25j) \times 10^9$	$\pm 1.32j \times 10^9$
9, 10	$(-0.02 \pm 6.81j) \times 10^9$	$\pm 6.81j \times 10^9$

(b)

i	$p_{L,i}$	$z_{L,i}$
1	-6.71×10^8	0
2, 3	$(-0.05 \pm 3.37j) \times 10^9$	$\pm 3.38j \times 10^9$
4, 5	$(-0.00 \pm 1.01j) \times 10^{10}$	$\pm 1.01j \times 10^{10}$
6	-4.35×10^8	0
7, 8	$(-0.16 \pm 1.25j) \times 10^9$	$\pm 1.32j \times 10^9$
9, 10	$(-0.02 \pm 6.76j) \times 10^9$	$\pm 6.76j \times 10^9$

For $M = 1$, Figure 4 compares Bound 1 (left y-axis) with Bound 3 (right y-axis) for the parallel dipoles when d varies from 0.03λ to 1.5λ. The horizontal dotted line indicates the limiting values as the dipoles become decoupled. Both curves show similar trends when the dipoles are closely spaced, and suggest a bandwidth peak at 0.24λ. For $d > 0.32\lambda$, the curves seem out of phase with each other. Further exploration is needed to see if there is any physical significance to this.

D. Rational approximation of time delays

Any characterization of physically separated antennas should account for the time of propagation of the signal between the antennas. Time delays associated with this distance can be modeled as a non-rational (exponential) function of s.

A simple idealized analytical model of time delay is shown in Figure 5, which consist of two RC loads and a coupling branch between them. The coupling is capacitive and includes a delay component. We examine our ability to match to this load in the 100–400 MHz band. As a reference value, without the time delay (zero delay), the S-matrix of the loads is real-rational and satisfies $S_L(\infty) = -I$, has two poles at -8.00×10^8 and -4.44×10^8, and has a zero at 0 with multiplicity two. We apply Bound 3 and obtain $B = 9.77 \times 10^8$.

In order to apply the broadband bounds to Figure 5, we need to approximate the delay using a rational function. We

consider two ways of doing this. The first way models the time delay term $e^{-5\times10^{-10}s}$ using the Padé approximation. We use the fraction

$$\frac{s^4-2\times10^{10}s^3+1.8\times10^{20}s^2-8.4\times10^{29}s+1.68\times10^{39}}{s^4+2\times10^{10}s^3+1.8\times10^{20}s^2+8.4\times10^{29}s+1.68\times10^{39}}.$$

This fraction is then inserted in place of the time delay, thus making the rational matrix $S_L(s)$ that satisfies $S_L(\infty) = -I$, and has poles and zeros shown in Table II(a). (We omit the expression of $S_L(s)$ because of its complexity.) Compared with the true S-matrix of the loads, the rational S-matrix has an average error of -119 dB in its entries between 100 MHz and 400 MHz. We apply Bound 3 and obtain 1.24×10^9. Using (9) with $\tau = 0.2$, we obtain $\delta B \approx 9.64 \times 10^7$, which is 8% of the bound. Hence (6) is

$$\int_{1\times10^8}^{4\times10^8} \log \frac{1}{r'(\omega)} d\omega \leq 1.34 \times 10^9. \tag{12}$$

This bound is larger than without the delay.

A second way to model delay is to avoid the analytical Padé step, and directly fit numerical simulations using rational matrices. To illustrate this, we treat the loads in Figure 5 as a black box, obtain a numerical frequency response, and use the Matrix Fitting Toolbox to fit this response. We use ten poles and ten zeros to fit the loads in 100–400 MHz, and enforce $S_L(\infty) = -I$. The resulting $S_L(s)$ has poles and zeros shown in Table II(b); the average error between the entries true S-matrix of the loads and entries of $S_L(s)$ is -150 dB. Bound 3 is applied to the fitted rational model, which yields $B = 1.24 \times 10^9$, and $\delta B \approx 1.75 \times 10^7$, which is 1% of the bound. The total is $B + \delta B = 1.26 \times 10^9$. This numerically fitted model result is similar to the Padé approximation result (12), illustrating the robustness of this approach.

In the next section, we further illustrate the numerical method by fitting loads that include sections of realistic transmission lines. No analytical modeling is needed.

E. Four commercial 2.5 GHz antennas

We consider a system where $M = N = 4$, and the loads consist of two pairs of Skycross iMAT-1115 commercial antennas designed for 2.5 GHz. The antennas are shown in Figure 6(a), numbered 1 through 4 from left to right. These antennas are simulated using Ansys HFSS in 2–4 GHz, and their de-embedded S-matrix $S'_L(j\omega)$ entries are plotted in Figure 6(b). The de-embedding removes the effect of the grounded coplanar feed lines that drive the antennas in the simulation. Each antenna in Figure 6(a) is one-tenth of a wavelength away from its neighbor at 2.5 GHz and the antennas therefore couple. From Figure 6(b), we see that antennas 1 and 2 are decoupled at 2.5 GHz, but not at other frequencies; antennas 2 and 3 have significant coupling near 2.5 GHz. We wish to examine the achievable bandwidth performance of these four antennas.

We apply the modeling method in Section II to the simulated $S'_L(j\omega)$. Figure 6(b) compares the simulated $S'_L(j\omega)$ with the $S_L(s)$; the expressions for $S_L(s)$ are not shown. The maximum of any element of $S_L(j\omega) - S'_L(j\omega)$ in 2–4 GHz is -38 dB, and the average over the frequency band is -53 dB. The $p_{L,i}$, $z_{L,i}$ for the antennas are listed in Table III. It is readily checked that $\det S_L(0) = 1$, and (1) is satisfied at $s_0 = 0$. Bound 1 yields

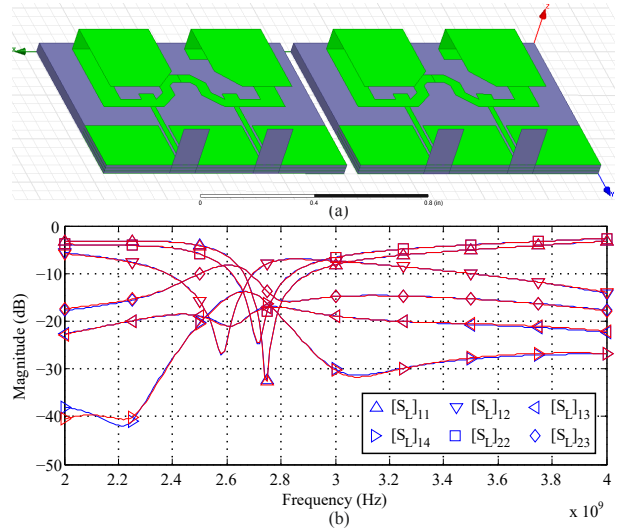

Fig. 6. (a) Geometries of two pairs of Skycross iMAT-1115 antennas. (b) The simulated and modeled S-matrix elements of the antennas versus frequency in 2–4 GHz. The HFSS simulated result $S'_L(j\omega)$ is shown in blue, and are compared with $S_L(j\omega)$ in red. Different elements are distinguished by different markers in the plot; only some of the elements in the S-matrix are shown because of the symmetry in the structure of the antennas.

TABLE III
VALUES OF $p_{L,i}$ AND $z_{L,i}$ FOR THE S-MATRIX OF THE ANTENNAS IN FIGURE 6(A).

i	$p_{L,i}$	$z_{L,i}$
1	-1.54×10^8	1.64×10^8
2	-7.74×10^9	3.67×10^{10}
3, 4	$(-0.43 \pm 1.37j) \times 10^{10}$	$(-0.23 \pm 2.23j) \times 10^{10}$
5, 6	$(-0.15 \pm 1.60j) \times 10^{10}$	$(-0.22 \pm 1.69j) \times 10^{10}$
7, 8	$(-0.08 \pm 1.69j) \times 10^{10}$	$(0.04 \pm 1.70j) \times 10^{10}$
9, 10	$(-0.75 \pm 2.40j) \times 10^{10}$	$(2.65 \pm 3.46j) \times 10^{10}$
11, 12	$(-0.40 \pm 3.14j) \times 10^{10}$	$(0.03 \pm 1.63j) \times 10^{10}$

$$\int_{\omega_1}^{\omega_2} \omega^{-2} \log \frac{1}{r(\omega)} d\omega \leq 2.31 \times 10^{-10}, \tag{13}$$

where $\omega_1 = 4\pi \times 10^9$ and $\omega_2 = 8\pi \times 10^9$.

We apply the steps in Section II-B to estimate δB for $\tau = 0.2$. The integral in (9) with $f(\omega) = 1/\omega^2$ yields $\delta B \approx 7.88 \times 10^{-11}$, which is equal to 34% of the bound in (13), and which we accept. Therefore,

$$\int_{\omega_1}^{\omega_2} \omega^{-2} \log \frac{1}{r'(\omega)} d\omega \leq B + \delta B = 3.10 \times 10^{-10} \tag{14}$$

is our bound for the four antennas.

The right-hand side of (14) is compared with the achieved bandwidth of two different matching networks. The first network is shown in Figure 7(a) for a single antenna; this network is duplicated four times, one for each antenna, and does not account for any antenna coupling. The second network, shown in Figure 7(b), is a decoupling network at 2.5 GHz designed using Method 4 in [21]. The achieved integral for the two networks are 6.98×10^{-12} and 2.49×10^{-11}, respectively.

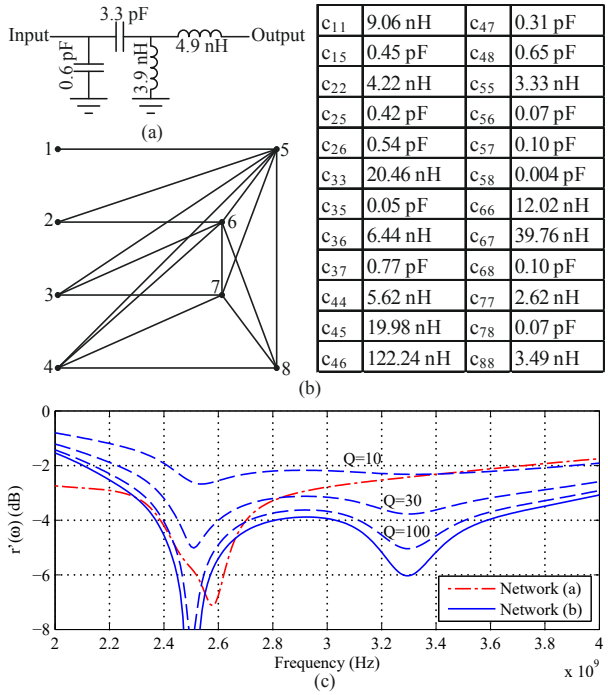

c_{11}	9.06 nH	c_{47}	0.31 pF
c_{15}	0.45 pF	c_{48}	0.65 pF
c_{22}	4.22 nH	c_{55}	3.33 nH
c_{25}	0.42 pF	c_{56}	0.07 pF
c_{26}	0.54 pF	c_{57}	0.10 pF
c_{33}	20.46 nH	c_{58}	0.004 pF
c_{35}	0.05 pF	c_{66}	12.02 nH
c_{36}	6.44 nH	c_{67}	39.76 nH
c_{37}	0.77 pF	c_{68}	0.10 pF
c_{44}	5.62 nH	c_{77}	2.62 nH
c_{45}	19.98 nH	c_{78}	0.07 pF
c_{46}	122.24 nH	c_{88}	3.49 nH

Fig. 7. (a) A two-port matching network for a single Skycross iMAT-1115 antenna (duplicated four times) that does not account for antenna coupling. (b) A decoupling network at 2.5 GHz designed using Method 4 in [21], where each line represents a capacitor or inductor, and each port is grounded through a component not drawn in figure. The capacitance and inductance values are listed in the table to the right; c_{ii} $i = 1, \ldots, 8$ are the components connecting port i to ground, and c_{ij} $i \neq j = 1, \ldots, 8$ are the components connecting port i and j. (c) The $r(\omega)$ for networks (a) and (b) are shown in 2–4 GHz. Also plotted is $r(\omega)$ for (b) when the reactive components have Q factors 10, 30 and 100.

Although the decoupling network has a better bandwidth performance than the network in Figure 7(a), there still exists a significant gap between the achieved integrals and (14), indicating that much better bandwidth performance with these antennas is still possible. The $r'(\omega)$ for both networks is plotted in Figure 7(c), where we see narrow bandwidth for both networks. Neither network comes close to achieving the desired threshold of $\tau = 0.2$ (power reflection ratio -14 dB) over 2–4 GHz, which should be possible according to (14). The design of a network to achieve (14) remains an open problem.

The reactive components in Figure 7(b) are ideal in that they have no resistive properties. To illustrate the bandwidth lost when the components have finite Q factors, we let the reactive components behave as ideal reactive components in parallel with resistances. All of the components in Figure 7(b) are assumed to have the same Q factors for all frequency, where Q is defined as the ratio between the susceptance and the conductance of the components. Figure 7(c) shows the $r'(\omega)$ for different Q factors.

Finally, we show that the grounded coplanar waveguide feed lines used for these antennas have minimal effect on the bound. We modify the S-matrix generated by Ansys HFSS by not de-embedding it from the transmission lines, thus including them in the frequency analysis. This S-matrix is then subjected to

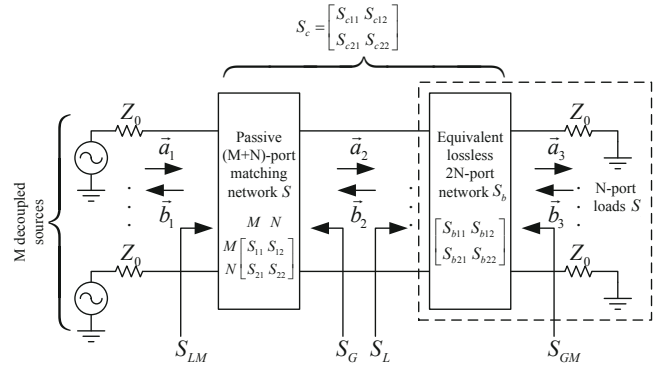

Fig. 8. An RF system where M uncorrelated sources drive N loads having S-matrix S_L through a passive $(M+N)$-port matching network S (the complex-frequency argument s is omitted). The N loads are shown in the dashed box using their equivalent Darlington representation, which consists of a lossless $2N$-port network S_b connected with N characteristic impedances Z_0. S_c is the $(M+N) \times (M+N)$ S-matrix of the concatenated network of S and S_b. S_{LM}, S_G and S_{GM} are the S-matrices as seen at different ports of the system.

standard rational fitting: We employ the Matrix Fitting Toolbox to fit the antennas using a rational matrix with 15 poles and zeros, and enforce (1) at $s_0 = 0$. We omit the details, but the result of Bound 1 is $B = 2.74 \times 10^{-10}$. From (9), $\delta B \approx 3.61 \times 10^{-11}$, and the result is $B + \delta B = 3.10 \times 10^{-10}$, which coincides with (14). Hence, the feed lines in this example do not affect the bandwidth, likely because they are equal in length and have minimal coupling between them.

We now provide derivations of the bounds used in both Parts of this paper.

IV. Derivations of Broadband Matching Bounds

The bounds are corollaries of Theorems 2 and 3, which are presented in Section IV-B. The presentation of the theorems requires the Darlington representation for multiport loads, which is itself presented in Section IV-A. The bounds are derived in Section IV-C.

A. Darlington equivalent network

We consider the RF system shown in Figure 8, where M uncorrelated sources drive N loads through a passive $(M+N)$-port matching network. The network has an $(M+N) \times (M+N)$ S-matrix $S(s)$ partitioned as

$$S(s) = \begin{array}{c} \\ M \\ N \end{array} \begin{array}{c} \begin{array}{cc} M & N \end{array} \\ \begin{pmatrix} S_{11}(s) & S_{12}(s) \\ S_{21}(s) & S_{22}(s) \end{pmatrix} \end{array}.$$

In Figure 8, we transform the N dissipative real loads $S_L(s)$ into an equivalent lossless real $2N$-port network $S_b(s)$ terminated by N isolated characteristic impedances Z_0. In [20], Darlington first verified that such an equivalent transformation is possible for $N = 1$. The extension to $N > 1$ is shown in [23]–[26]. The fact that $I - S_L^T(-s)S_L(s)$ has full normal rank ensures that there are N resistors in the Darlington network [25, III.3.1].

We partition the $2N \times 2N$ S-matrix $S_b(s)$ as

$$S_b(s) = \begin{bmatrix} S_{b11}(s) & S_{b12}(s) \\ S_{b21}(s) & S_{b22}(s) \end{bmatrix},$$

where $S_{bij}(s)$ are $N \times N$ submatrices. Then the necessary and sufficient condition for $S_b(s)$ being a Darlington equivalent network for a real-rational $S_L(s)$ is that $S_b(s)$ is real-rational, Hurwitzian, bounded and para-unitary, and $S_{b11}(s) = S_L(s)$. We do not need to know the exact form of the rest of $S_b(s)$, only its existence is needed.

In Figure 8, let $S_c(s)$ be the $(M+N) \times (M+N)$ S-matrix of the concatenated network of $S(s)$ and $S_b(s)$, partitioned as

$$S_c(s) = \begin{array}{c c} & \begin{array}{cc} M & N \end{array} \\ \begin{array}{c} M \\ N \end{array} & \begin{pmatrix} S_{c11}(s) & S_{c12}(s) \\ S_{c21}(s) & S_{c22}(s) \end{pmatrix} \end{array}.$$

Let $S_{GM}(s)$ be the $N \times N$ S-matrix seen from the output ports of $S_b(s)$, and $S_G(s)$ be the $N \times N$ S-matrix seen from the output ports of $S(s)$. It follows that $S_G(s) = S_{22}(s)$, $S_{GM}(s) = S_{c22}(s)$, and

$$S_{GM}(s) = S_{b22}(s) + S_{b21}(s)S_G(s)(I - S_L(s)S_G(s))^{-1}S_{b12}(s). \quad (15)$$

We use the notation $p_{\times,i}$ and $z_{\times,i}$, $i = 1, 2, \ldots$ to represent the poles and zeros over the WCP of $S_\times(s)$, where $S_\times$ is any of the S-matrices or submatrices shown in Figure 8. In addition, we use the subscript "+" to denote the zeros or poles that are in the RHP, and "−" to denote those in the LHP.

In Figure 8, let $\vec{a}_3(s)$ and $\vec{b}_3(s)$ be the $N \times 1$ incident and reflected signal to and from the isolated impedances Z_0. Because $S_b(s)$ is lossless, the amount of power delivered to the loads equals the power delivered to the resistive part of the Darlington network. Since $\vec{b}_3(j\omega) = 0$, the power delivered at $j\omega$ is $\|\vec{a}_3(j\omega)\|^2$, where $\vec{a}_3(j\omega) = S_{c21}(j\omega)\vec{a}_1(j\omega)$. So the total power lost to reflection and dissipation can be written as $\|\vec{a}_1(j\omega)\|^2 - \|\vec{a}_3(j\omega)\|^2$, and the power loss ratio of the matching network and the loads becomes

$$r^2(\omega) = 1 - \frac{1}{M}\text{tr}\{S_{c21}^H(j\omega)S_{c21}(j\omega)\}. \quad (16)$$

In the rest of the presentation, we use a particular Darlington network, which is given in the following lemma in [9].

Lemma 1: There exists a Darlington network $S_b(s)$ such that

$$z_{b22+,i} = -z_{L-,i}. \quad (17)$$

For such $S_b(s)$, the RHP zeros of $S_{GM}(s)$ are identical to the RHP zeros of $S_L^T(-s) - S_G(s)$.

B. Integral log-determinant of $S_{GM}(j\omega)$

We now present the theorems on the integral of logarithm of $\det S_{GM}(j\omega)$. We assume that $I - S_L^T(-s)S_L(s)$ is full normal rank. We also assume (1) is satisfied for some $\text{Re}\{s_0\} \geq 0$, and choose positive integer m such that

$$I - S_L^T(-s)S_L(s) = A_m(s - s_0)^m + A_{m+1}(s - s_0)^{m+1} + \ldots \quad (18)$$

if s_0 is finite, or

$$I - S_L^T(-s)S_L(s) = A_m s^{-m} + A_{m+1}s^{-(m+1)} + \ldots \quad (19)$$

if $s_0 = \infty$. In (18) and (19), $A_m \neq 0$ is defined such that the entries of $I - S_L^T(-s)S_L(s)$ have a zero at $s = s_0$ with multiplicity at least m. When $s_0 = j\omega_0$, it is shown in Lemma 4 in Appendix C that m is even; when $s_0 = \infty$, m is also even since the left-hand side of (19) is an even function. The general broadband matching theorems are as follows:

Theorem 2: Let $S_L(s)$ satisfy (18) for some $\text{Re}\{s_0\} \geq 0$. Then for any passive network $S(s)$ such that $I - S_L(s_0)S_G(s_0)$ is non-singular, we have

$$\int_0^\infty \text{Re}[(s_0 - j\omega)^{-1} + (s_0 + j\omega)^{-1}] \log|\det S_{GM}(j\omega)| d\omega = \pi \log\left|\det S_L(s_0) \cdot \frac{\prod_i (s_0 + z_{L,i}) \prod_i (s_0 + z_{GM+,i})}{\prod_i (s_0 - z_{L,i}) \prod_i (s_0 - z_{GM+,i})}\right|, \quad (20)$$

and

$$\int_0^\infty [(s_0 - j\omega)^{-(k+1)} + (s_0 + j\omega)^{-(k+1)}] \times \log|\det S_{GM}(j\omega)| d\omega = \frac{(-1)^k \pi}{k}\Big[\sum_i (p_{L,i} - s_0)^{-k} - \sum_i (-z_{L,i} - s_0)^{-k} + \Big(\sum_i (z_{GM+,i} - s_0)^{-k} - \sum_i (-z_{GM+,i} - s_0)^{-k}\Big)\Big] \quad (21)$$

for $k = 1, \ldots, m-1$, where $\pm s_0$, $\pm s_0^*$ are excluded in $p_{L,i}$, $z_{L,i}$ in (21). If $I - S_L(s_0)S_G(s_0)$ is singular, then $\text{Re}\{s_0\} = 0$, (20) holds, and (21) holds for $k = 1, \ldots, m-2$; for $k = m-1$, we let $s_0 = j\omega_0$, and then have

$$\int_0^\infty [(\omega_0 - \omega)^{-m} + (\omega_0 + \omega)^{-m}] \log|\det S_{GM}(j\omega)| d\omega \geq \frac{(-1)^{\frac{m-2}{2}} \pi}{m-1}\Big[\sum_i (p_{L,i} - j\omega_0)^{-(m-1)} - \sum_i (-z_{L,i} - j\omega_0)^{-(m-1)} + \Big(\sum_i (z_{GM+,i} - j\omega_0)^{-(m-1)} - \sum_i (-z_{GM+,i} - j\omega_0)^{-(m-1)}\Big)\Big]. \quad (22)$$

Theorem 3: Let $S_L(s)$ satisfy (19). Then

$$\int_0^\infty \omega^{k-1} \log|\det S_{GM}(j\omega)| d\omega \geq \frac{(-1)^{\frac{k-1}{2}} \pi}{2k}\Big[\sum_i p_{L,i}^k + \sum_i z_{L,i}^k + 2\sum_i z_{GM+,i}^k\Big] \quad (23)$$

for $k = 1, 3, \ldots, m-1$. Equality in (23) holds if $k \neq m-1$ or $I - S_L(s)S_G(s)$ is non-singular at $s = \infty$.

In Theorem 2, although (18) holds, s_0 may still be a zero of $S_L(s)$ when $\text{Re}\{s_0\} > 0$. This happens if and only if $S_L(s)$ has a pole at $-s_0$, which cancels the zero at s_0 in (18). Hence, the poles and zeros of $S_L(s)$ at $\pm s_0$, $\pm s_0^*$ are excluded in the sums in (21). The proof of Theorem 2 appears

in Appendix D; the proof uses several preliminary lemmas which are introduced in Appendices B and C.

Theorem 3 is adapted from Theorem 1 in [9], which is proven with $\det S_{LM}(j\omega)$ in place of $\det S_{GM}(j\omega)$ in (23). Note $S_{LM}(s)$ is the $M \times M$ S-matrix seen from the input ports of $S(s)$ (see Figure 8). Although it is assumed in [9] that $M = N$, and that the matching network is lossless and reciprocal, and the loads are also reciprocal, these assumptions can be relaxed. In fact, Theorem 1 in [9] applies without change to non-reciprocal networks and loads; the reciprocity of the networks and loads is an unnecessary restriction in the model. Our version is needed to handle lossy networks, which are not handled in [9]. The proof of (23) follows the same arguments used in the proof of Theorem 2 and is omitted.

C. Proof of bounds

We relate $\det S_{GM}(j\omega)$ to $r(\omega)$ in (16) using the arithmetic-geometric mean inequality:

$$\begin{aligned} r^2(\omega) &= \frac{1}{M}\mathrm{tr}\{I - S_{c21}^H(j\omega)S_{c21}(j\omega)\} \\ &\geq \det(I - S_{c21}(j\omega)S_{c21}^H(j\omega))^{1/M} \\ &\geq \det(S_{GM}(j\omega)S_{GM}^H(j\omega))^{1/M} = |\det S_{GM}(j\omega)|^{2/M}. \end{aligned}$$

The first equality holds if and only if the eigenvalues of $I - S_{c21}^H(j\omega)S_{c21}(j\omega)$ are all equal; this is equivalent to $S_{21}^H(I - S_G S_L)^{-H}(I - S_L^H S_L)(I - S_G S_L)^{-1}S_{21}$ having equal singular values for all $j\omega$, which is Condition 2 for equality in [1]. The second equality holds if and only if $S(s)$ satisfies $S_{c21}(s)S_{c21}^T(-s) + S_{GM}(s)S_{GM}^T(-s) = I$. Since $S_b(s)$ is para-unitary, this is equivalent to $S_{21}(s)S_{21}^T(-s) + S_G(s)S_G^T(-s) = I$, which is Condition 1.

Taking the logarithm on both sides of the inequality yields

$$\log r(\omega) \geq (1/M)\log|\det S_{GM}(j\omega)|. \tag{24}$$

When $s_0 = j\omega_0$, we apply (24) to (21) and (22) for $k = 1$, and omit $\sum_i (z_{GM+,i} - j\omega_0)^{-1} - \sum_i (-z_{GM+,i} - j\omega_0)^{-1}$ since it is non-negative. From Lemma 1, the RHP zeros of $S_{GM}(s)$ are identical to the RHP zeros of $S_L^T(-s) - S_G(s)$; thus Condition 4 is necessary and one of the sufficient conditions. This finishes the proof of Bound 1.

When $\mathrm{Re}\{s_0\} > 0$, we apply (24) to (20), and then omit $\frac{\prod_i (s_0 + z_{GM+,i})}{\prod_i (s_0 - z_{GM+,i})}$ since it has modulus no smaller than one. Note $\mathrm{Re}[(s_0 - j\omega)^{-1} + (s_0 + j\omega)^{-1}]$ in (20) is positive for any $\mathrm{Re}\{s_0\} > 0$ and ω. The result is Bound 2.

We combine (24) and (23) for $k = 1$, and then omit $\sum_i z_{GM+,i}$ since it is non-negative. The result is Bound 3. ■

V. Conclusions and Future Work

We have presented a bandwidth analysis for multiport matching that applies to an arbitrary number of sources and coupled loads, using broadband matching bounds on the integral of a power loss ratio. Part I presented the definitions and bounds and applied them to settings where the loads could be described analytically using rational functions. Conditions were given for when the bounds could be met with equality. Part II focused on realistic loads, including antennas, and the rational fitting needed for accurate bandwidth calculations. Proofs of all results were also presented.

Part I demonstrated that the bound scales generally as N/M for M sources and N loads. This scaling is not affected by coupling as long as it is not "too strong". Hence, large bandwidth is possible even if the loads are coupled or closely-spaced. Some realistic examples in Part II showed how large bandwidths can be attained in practice. Although we touched upon techniques to attain the bounds, the general practical design problem remains open.

For loads, such as antennas, whose frequency responses are available numerically through simulation, rational fitting of the S-matrix is required to apply the bounds. We showed how the rational matrix is then used to find a bandwidth bound for the system being fitted. Increasing the polynomial orders of the numerators and denominators of the rational functions in the S-matrix generally improves the accuracy of the system approximation, but can cause the problem of over-fitting, which results in a loose bound. Over-fitting is an important issue that deserves further attention.

Our examples included antennas that are matched near their resonant frequency. It would be interesting to see how the bounds characterize the bandwidth for electrically small antennas, which are being used below their resonant frequencies and are generally considered narrowband. The classical Chu bound [28] and some recent advances [29]–[31] provide other methods to describe the bandwidth for small antennas. One future area of study could be to reconcile these methods with bandwidth results calculated using the modeling techniques and bounds contained herein.

The communication-theoretic implications of using broadband multiport networks in wireless systems need study. We have been concerned primarily with the aspects of network design that ensure efficient power delivery to loads such as an array of multiple coupled antennas. However, the choice of network can also affect the radiation efficiency and far-field pattern of an antenna array. Hence, a complete system design should consider total power transfer from the transmitter amplifiers to a far-field receiver. We also did not examine the implications of using the wideband matching networks for antennas that are intended for both transmission and reception.

Although we have treated the case where uncorrelated sources are driving coupled loads, the reverse situation where coupled sources are driving decoupled loads needs separate analysis. Such a system could arise when the sources are closely-spaced receiver antennas connected to isolated low-noise amplifiers. The noise figures of the amplifiers would play a role in the criterion for determining bandwidth.

Maximizing the data rate attainable with a prescribed set of N antennas is a potentially interesting problem. Conventional narrowband Shannon theory says that MIMO, with M independent data streams (sources) in a rich scattering environment, achieves rates linear in N when $M = N$ [32]. But, as we have seen, the bandwidth attainable for $M = N$ is only $1/N$ of that attainable for $M = 1$. Thus, MIMO with N streams achieves $1/N$ the bandwidth of MIMO with a single stream. Since the transmission data rate is directly

proportional to bandwidth, one could therefore conjecture that, with N antennas, one stream is as good as N. This bandwidth/multiplexing trade-off needs further study.

VI. Acknowledgements

We thank the reviewers and editor for the detailed and insightful comments on both parts of our manuscript. In particular, your technical suggestions on how to improve the readability of the paper helped us to treat the issues of the experimental determination of $r(\omega)$, and the rational fitting of realistic loads.

Appendix

Theorem 1 is proven in Appendix A. We prove Theorem 2 in Appendix D using several preliminary lemmas that are introduced in Appendices B and C.

A. Proof of Theorem 1

Let $\varepsilon(\omega) = r^2(\omega) - r'^2(\omega)$. Then

$$\int_{\omega_1}^{\omega_2} f(\omega)\log\frac{r(\omega)}{r'(\omega)}d\omega = \int_{\omega_1}^{\omega_2}\frac{f(\omega)}{2}\log\left(1+\frac{\varepsilon(\omega)}{r'^2(\omega)}\right)d\omega$$
$$= \int_{\omega_1}^{\omega_2}\frac{f(\omega)}{2}\log\left(1+\frac{1-r'^2(\omega)}{r'^2(\omega)}\cdot\frac{\varepsilon(\omega)}{1-r'^2(\omega)}\right)d\omega.$$

We show that $\varepsilon(\omega)/(1-r'^2(\omega)) \le \rho(\omega)$.

From (5) in Part I,

$$r^2(\omega) = 1- \frac{\mathrm{tr}\{S_{21}^H(I-S_GS_L)^{-H}(I-S_L^HS_L)(I-S_GS_L)^{-1}S_{21}\}}{M},$$

and a similar relation between $r'^2(\omega)$ and $S'_L(j\omega)$ holds. For simplicity of the presentation, we omit the argument $j\omega$ for the S-matrices in the remainder of the proof. We perturb $S_L(j\omega) = S'_L(j\omega) + \delta S_L(j\omega)$; a first-order expansion yields

$$\varepsilon(\omega) = r^2(\omega) - r'^2(\omega) \approx -\frac{1}{M}\mathrm{tr}\{S_{21}^H(I-S_GS'_L)^{-H}A_1(I-S_GS'_L)^{-1}S_{21}\},$$

where A_1 is the Hermitian matrix

$$A_1 = \delta S_L^H(I-S'_LS_G)^{-H}(S_G^H - S'_L) + (S_G - S_L'^H)(I-S'_LS_G)^{-1}\delta S_L.$$

Because A_1 is Hermitian, the matrix $S_{21}^H(I-S_GS'_L)^{-H}A_1(I-S_GS'_L)^{-1}S_{21}$ is also Hermitian. Some manipulations of the trace give us

$$\varepsilon(\omega) \le \frac{\sigma_{1,\max}}{M}\mathrm{tr}\{S_{21}^H(I-S_GS'_L)^{-H}(I-S_GS'_L)^{-1}S_{21}\},$$

where $\sigma_{1,\max}$ is the maximum singular value of A_1. Similarly,

$$1-r'^2(\omega) = \frac{1}{M}\mathrm{tr}\{S_{21}^H(I-S_GS'_L)^{-H}(I-S_L'^HS'_L)(I-S_GS'_L)^{-1}S_{21}\} \ge \frac{1-\sigma_{L,\max}'^2(\omega)}{M}\mathrm{tr}\{S_{21}^H(I-S_GS'_L)^{-H}(I-S_GS'_L)^{-1}S_{21}\}.$$

Hence,

$$\frac{\varepsilon(\omega)}{1-r'^2(\omega)} \le \frac{\sigma_{1,\max}}{1-\sigma_{L,\max}'^2(\omega)}.$$

We now seek an upper bound on $\sigma_{1,\max}$, which depends on the maximum singular values of both δS_L and $(S_G - S_L'^H)(I-S'_LS_G)^{-1}$. The maximum singular value of δS_L is $\sigma_{\delta,\max}(\omega)$. To obtain the maximum singular value of $(S_G - S_L'^H)(I-S'_LS_G)^{-1}$, we try to prove that

$$I + (\sigma_{L,\max}'^2(\omega) - \sigma_{L,\min}'^2(\omega))(I-S'_LS_G)^{-H}(I-S'_LS_G)^{-1} - (I-S'_LS_G)^{-H}(S_G^H - S'_L)(S_G - S_L'^H)(I-S'_LS_G)^{-1} \tag{25}$$

is a positive semidefinite matrix, which means the maximum eigenvalue of the positive definite matrix $I + (\sigma_{L,\max}'^2(\omega) - \sigma_{L,\min}'^2(\omega))(I-S'_LS_G)^{-H}(I-S'_LS_G)^{-1}$ is larger than or equal to the maximum eigenvalue of the positive semidefinite matrix $(I-S'_LS_G)^{-H}(S_G^H - S'_L)(S_G - S_L'^H)(I-S'_LS_G)^{-1}$. Then the square root of the maximum eigenvalue of $I + (\sigma_{L,\max}'^2(\omega) - \sigma_{L,\min}'^2(\omega))(I-S'_LS_G)^{-H}(I-S'_LS_G)^{-1}$ is larger than or equal to the maximum singular value of $(S_G - S_L'^H)(I-S'_LS_G)^{-1}$.

To prove that (25) is positive semidefinite, we simplify it

$$I + (\sigma_{L,\max}'^2(\omega) - \sigma_{L,\min}'^2(\omega))(I-S'_LS_G)^{-H}(I-S'_LS_G)^{-1} - (I-S'_LS_G)^{-H}(S_G^H - S'_L)(S_G - S_L'^H)(I-S'_LS_G)^{-1} = (I-S'_LS_G)^{-H}A_2(I-S'_LS_G)^{-1},$$

where

$$A_2 = (\sigma_{L,\max}'^2(\omega) - \sigma_{L,\min}'^2(\omega))I + (I - S'_LS_L'^H) - S_G^H(I - S_L'^HS'_L)S_G.$$

A_2 is a positive semidefinite matrix because the singular values of S'_L and S_G are no larger than one, and therefore the minimum eigenvalue of the positive definite matrix $(\sigma_{L,\max}'^2(\omega) - \sigma_{L,\min}'^2(\omega))I + (I - S'_LS_L'^H)$ is larger than or equal to the maximum eigenvalue of the positive semidefinite matrix $S_G^H(I - S_L'^HS'_L)S_G$. Therefore, we have proven that the square root of the maximum eigenvalue of $I + (\sigma_{L,\max}'^2(\omega) - \sigma_{L,\min}'^2(\omega))(I-S'_LS_G)^{-H}(I-S'_LS_G)^{-1}$ is larger than or equal to the maximum singular value of $(S_G - S_L'^H)(I-S'_LS_G)^{-1}$. The maximum eigenvalue of $I + (\sigma_{L,\max}'^2(\omega) - \sigma_{L,\min}'^2(\omega))(I-S'_LS_G)^{-H}(I-S'_LS_G)^{-1}$ is smaller than or equal to $1 + \frac{\sigma_{L,\max}'^2(\omega) - \sigma_{L,\min}'^2(\omega)}{(1-\sigma'_{L,\max}(\omega))^2}$. Therefore, the maximum singular value of $(S_G - S_L'^H)(I-S'_LS_G)^{-1}$ is smaller than or equal to $\sqrt{1 + \frac{\sigma_{L,\max}'^2(\omega) - \sigma_{L,\min}'^2(\omega)}{(1-\sigma'_{L,\max}(\omega))^2}}$. We conclude

$$\sigma_{1,\max} \le 2\sigma_{\delta,\max}(\omega)\sqrt{1 + \frac{\sigma_{L,\max}'^2(\omega) - \sigma_{L,\min}'^2(\omega)}{(1-\sigma'_{L,\max}(\omega))^2}},$$

which yields $\varepsilon(\omega)/(1-r'^2(\omega)) \le \rho(\omega)$. This finishes the proof. ■

B. Preliminary lemmas on real-rational functions

Lemma 2: Let $f(s)$ be a real-rational function with $f(s_0) = c \neq 0$. Then the series expansion of $\log f(s)$ around $s = s_0$ can be written as

$$\log f(s) = \log c + a_1(s - s_0) + a_2(s - s_0)^2 + \ldots + a_\ell(s - s_0)^\ell + \ldots, \tag{26}$$

where

$$a_\ell = \frac{1}{\ell}\left(\sum_i (p_i - s_0)^{-\ell} - \sum_i (z_i - s_0)^{-\ell}\right) \tag{27}$$

for $\ell = 1, 2, \ldots$, where p_i, z_i are the poles and zeros of $f(s)$.

Proof: Since $f(s_0) \neq 0$ is finite, $\log f(s_0) = \log c$ is finite. So the expansion of $\log f(s)$ around $s = s_0$ can be obtained using Taylor series expansion. The result is (27). ■

Lemma 3: Let $f(s)$ be a real-rational function. For any $\mathrm{Re}\{s_0\} \geq 0$, if $f(s_0)$ is finite, non-zero, and $1 - f(-s)f(s)$ has a zero at $s = s_0$ with multiplicity m, then

$$\int_0^\infty \mathrm{Re}[(s_0 - j\omega)^{-1} + (s_0 + j\omega)^{-1}] \log|f(j\omega)| d\omega = \pi \log\left|f(s_0)\frac{\prod_i (s_0 - p_{+,i}) \prod_i (s_0 + z_{+,i})}{\prod_i (s_0 + p_{+,i}) \prod_i (s_0 - z_{+,i})}\right|, \tag{28}$$

and

$$\begin{aligned}\int_0^\infty &[(s_0 - j\omega)^{-(k+1)} + (s_0 + j\omega)^{-(k+1)}] \log|f(j\omega)| d\omega \\ &= \frac{(-1)^k \pi}{k}\Big[\sum_i (p_i - s_0)^{-k} - \sum_i (z_i - s_0)^{-k} \\ &- \Big(\sum_i (p_{+,i} - s_0)^{-k} - \sum_i (-p_{+,i} - s_0)^{-k}\Big) \\ &+ \Big(\sum_i (z_{+,i} - s_0)^{-k} - \sum_i (-z_{+,i} - s_0)^{-k}\Big)\Big]\end{aligned} \tag{29}$$

for $k = 1, \ldots, m - 1$, where p_i, z_i are the poles and zeros of $f(s)$ in the WCP, and $p_{+,i}, z_{+,i}$ are the poles and zeros of $f(s)$ in the RHP.

Proof: Since $f(s_0) \neq 0$, we begin by applying Lemma 2 to write the expansion of $\log f(s)$ as (26) and (27). For convenience, we define another real-rational function $\hat{f}(s)$ as

$$\hat{f}(s) = f(s)\frac{\prod_i (s - p_{+,i})}{\prod_i (s + p_{+,i})}\frac{\prod_i (s + z_{+,i})}{\prod_i (s - z_{+,i})}, \tag{30}$$

where $p_{+,i}$ and $z_{+,i}$ are the poles and zeros of $f(s)$ in the RHP. Then $\hat{f}(s)$ has no poles or zeros in the RHP, and satisfies $\hat{f}(-s)\hat{f}(s) = f(-s)f(s)$ and $|\hat{f}(j\omega)| = |f(j\omega)|$. We apply Lemma 2 to $\hat{f}(s)$ and get

$$\log \hat{f}(s) = \log \hat{c} + \hat{a}_1(s - s_0) + \hat{a}_2(s - s_0)^2 + \ldots + \hat{a}_\ell(s - s_0)^\ell + \ldots, \tag{31}$$

where

$$\hat{c} = \hat{f}(s_0) = f(s_0)\frac{\prod_i (s_0 - p_{+,i})}{\prod_i (s_0 + p_{+,i})}\frac{\prod_i (s_0 + z_{+,i})}{\prod_i (s_0 - z_{+,i})}, \tag{32}$$

and

$$\hat{a}_\ell = a_\ell - \frac{1}{\ell}\left(\sum_i (p_{+,i} - s_0)^{-\ell} - \sum_i (-p_{+,i} - s_0)^{-\ell}\right) + \frac{1}{\ell}\left(\sum_i (z_{+,i} - s_0)^{-\ell} - \sum_i (-z_{+,i} - s_0)^{-\ell}\right). \tag{33}$$

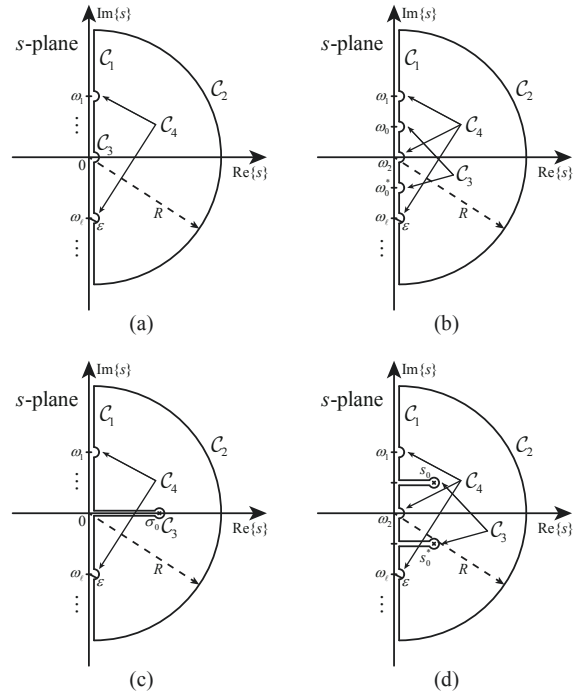

Fig. 9. The contours for the integrals (35), (37), (39) and (41) are shown in (a)–(d), respectively. The contours are in the clockwise direction. The sections of the contours are labeled $\mathcal{C}_1, \mathcal{C}_2, \ldots$ and their detailed descriptions are given in the proof of Lemma 3.

We can expand $\log f(s)$ and $\log \hat{f}(s)$ at $s = s_0^*$ in similar forms as (26) and (31). Since $f(s)$ and $\hat{f}(s)$ are real-rational, the coefficients for the expansion of $\log f(s)$ and $\log \hat{f}(s)$ at $s = s_0^*$ are a_ℓ^* and $\hat{a}_\ell^*$, respectively.

The next step is to separate our discussions into four cases: $s_0 = 0$, $j\omega_0$, σ_0, $\sigma_0 + j\omega_0$. Since the cases are similar to one another, we elaborate more on the $s_0 = 0$ case than the others.

1) $s_0 = 0$: Since $1 - f(-s)f(s)$ is an even real-rational function and has a zero of multiplicity m at $s_0 = 0$, m must be an even integer. We take the logarithm of $\hat{f}(-s)\hat{f}(s) = f(-s)f(s) = 1 + O(s^m)$ and use the expansion (31) at $s_0 = 0$. Because $\hat{f}(s)$ is real-rational, the coefficients in (33) for $s_0 = 0$ are real. We therefore obtain $|\hat{c}| = 1$, $\hat{a}_2 = \hat{a}_4 = \ldots = \hat{a}_{m-2} = 0$ and $\mathrm{Im}\{\hat{a}_1\} = \mathrm{Im}\{\hat{a}_3\} = \ldots = \mathrm{Im}\{\hat{a}_{m-1}\} = 0$.

For $s_0 = 0$, (28) is trivial since both sides are zero. Because $\hat{a}_2 = \hat{a}_4 = \ldots = \hat{a}_{m-2} = 0$, (29) is also trivial for $k = 2, 4, \ldots, m - 2$. We show (29) for $k = 1, 3, \ldots, m - 1$ by taking the contour integral of the function

$$s^{-(k+1)} \log \hat{f}(s) \tag{34}$$

along the closed curve shown in Figure 9(a). This function is analytic in the RHP; it is also analytic on the imaginary axis except the origin and possible zeros and poles of $\hat{f}(s)$ on the imaginary axis, which we denote as $j\omega_\ell$. Therefore, the following contour integral is zero:

$$\int_{\mathcal{C}_1 + \mathcal{C}_2 + \mathcal{C}_3 + \mathcal{C}_4} s^{-(k+1)} \log \hat{f}(s) ds = 0, \tag{35}$$

where $\mathcal{C}_1$ is the line segment between $-jR$ and jR excluding $[-\varepsilon,\varepsilon]$ and $[j(\omega_\ell-\varepsilon),j(\omega_\ell+\varepsilon)]$; $\mathcal{C}_2$ is the right semicircle with radius R centered at the origin; $\mathcal{C}_3$ is the right semicircle with radius ε centered at the origin; and $\mathcal{C}_4$ includes the right semicircles with radius ε centered at $j\omega_\ell$. We evaluate the integral of (34) as follows:

$$\int_{\mathcal{C}_1} s^{-(k+1)}\log\hat{f}(s)ds$$
$$=(-1)^{\frac{k+1}{2}}j\int_{-R}^{R}\omega^{-(k+1)}\log|f(j\omega)|d\omega-\frac{(-1)^{\frac{k+1}{2}}2\arg(\hat{c})}{k\varepsilon^k}$$
$$+O(R^{-k}),$$

where the integral from $-R$ to R excludes the intervals $[-\varepsilon,\varepsilon]$ and $[\omega_\ell-\varepsilon,\omega_\ell+\varepsilon]$. Furthermore,

$$\int_{\mathcal{C}_2} s^{-(k+1)}\log\hat{f}(s)ds=\int_{\pi/2}^{-\pi/2}j(Re^{j\theta})^{-k}\log\hat{f}(Re^{j\theta})d\theta$$
$$=O\left(\frac{\log R}{R}\right).$$

$$\int_{\mathcal{C}_3} s^{-(k+1)}\log\hat{f}(s)ds=\int_{-\pi/2}^{\pi/2}j(\varepsilon e^{j\theta})^{-k}\log\hat{f}(\varepsilon e^{j\theta})d\theta$$
$$=j\pi\hat{a}_k+\frac{(-1)^{\frac{k+1}{2}}2\arg(\hat{c})}{k\varepsilon^k}+O(\varepsilon^{m-k}).$$

$$\int_{\mathcal{C}_4} s^{-(k+1)}\log\hat{f}(s)ds=\sum_{\ell}\int_{-\pi/2}^{\pi/2}(j\omega_\ell+\varepsilon e^{j\theta})^{-(k+1)}$$
$$\times\log\hat{f}(j\omega_\ell+\varepsilon e^{j\theta})j\varepsilon e^{j\theta}d\theta=O(\varepsilon\log\varepsilon).$$

Combining these path integrals and letting $R\to\infty$, $\varepsilon\to 0$, we have

$$\int_{-\infty}^{\infty}\omega^{-(k+1)}\log|f(j\omega)|d\omega=(-1)^{\frac{k-1}{2}}\pi\hat{a}_k.$$

Since $f(s)$ is real-rational, $|f(-j\omega)|=|f^*(j\omega)|=|f(j\omega)|$, we have $\omega^{-(k+1)}\log|f(j\omega)|$ is an even function for $k=1,3,\ldots,m-1$. Using (33), we get (29) for $k=1,3,\ldots,m-1$. This finishes the proof for $s_0=0$.

2) $s_0=j\omega_0$: Since $1-f(-s)f(s)$ is a real-rational function and has a zero of multiplicity m at $s=j\omega_0$, it also has a zero of multiplicity m at $s=-j\omega_0$. We take the logarithm of $\hat{f}(-s)\hat{f}(s)=f(-s)f(s)=1+O((s-j\omega_0)^m)$ and use the expansion (31) at $s_0=j\omega_0$. We therefore obtain $|\hat{c}|=1$, $\mathrm{Im}\{a_1\}=\mathrm{Im}\{a_3\}=\ldots=\mathrm{Im}\{a_k\}=0$ for odd k and $k<m$, and $\mathrm{Re}\{a_2\}=\mathrm{Re}\{a_4\}=\ldots=\mathrm{Re}\{a_k\}=0$ for even k and $k<m$.

For $s_0=j\omega_0$, (28) is trivial since both sides are zero. We show (29) by taking the contour integral of the function

$$[(j\omega_0-s)^{-(k+1)}+(j\omega_0+s)^{-(k+1)}]\log\hat{f}(s) \tag{36}$$

along the closed curve shown in Figure 9(b). This function is analytic in the RHP; it is also analytic on the imaginary axis except $\pm j\omega_0$ and possible zeros and poles of $\hat{f}(s)$ on the imaginary axis, which we denote as $j\omega_\ell$. Therefore,

$$\int_{\mathcal{C}_1+\mathcal{C}_2+\mathcal{C}_3+\mathcal{C}_4}[(j\omega_0-s)^{-(k+1)}+(j\omega_0+s)^{-(k+1)}]$$
$$\times\log\hat{f}(s)ds=0, \tag{37}$$

where $\mathcal{C}_1$ is the line segment between $-jR$ and jR excluding $[j(\omega_0-\varepsilon),j(\omega_0+\varepsilon)]$, $[j(-\omega_0-\varepsilon),j(-\omega_0+\varepsilon)]$ and $[j(\omega_\ell-\varepsilon),j(\omega_\ell+\varepsilon)]$; $\mathcal{C}_2$ is the right semicircle with radius R centered at the origin; $\mathcal{C}_3$ includes the right semicircles with radius ε centered at the $j\omega_0$ and $-j\omega_0$; and $\mathcal{C}_4$ includes the right semicircles with radius ε centered at $j\omega_\ell$.

By evaluating the integral paths in (37), and letting $R\to\infty$, $\varepsilon\to 0$, we obtain

$$\int_{-\infty}^{\infty}[(\omega_0-\omega)^{-(k+1)}+(\omega_0+\omega)^{-(k+1)}]\log|f(j\omega)|d\omega$$
$$=(-1)^k j^{k+1}2\pi\hat{a}_k.$$

We have $[(\omega_0-\omega)^{-(k+1)}+(\omega_0+\omega)^{-(k+1)}]\log|f(j\omega)|$ is an even function, and using (33) we get (29) for $k=1,2,\ldots,m-1$. This finishes the proof for $s_0=j\omega_0$.

3) $s_0=\sigma_0$: Since $f(s)$ is a real-rational function, $\mathrm{Im}\{\hat{a}_1\}=\mathrm{Im}\{\hat{a}_2\}=\ldots=\mathrm{Im}\{\hat{a}_{m-1}\}=0$. For $s_0=\sigma_0$, we show (28) and (29) by taking the contour integral of the function

$$[(\sigma_0-s)^{-(k+1)}+(\sigma_0+s)^{-(k+1)}]\log\hat{f}(s) \tag{38}$$

along the close curve shown in Figure 9(c). This function is analytic in the RHP except σ_0; it is also analytic on the imaginary axis except possible zeros and poles of $\hat{f}(s)$ on the imaginary axis, which we denote as $j\omega_\ell$. Therefore, the following contour integral is zero for $k=0,1,2,\ldots,m-1$:

$$\int_{\mathcal{C}_1+\mathcal{C}_2+\mathcal{C}_3+\mathcal{C}_4}[(\sigma_0-s)^{-(k+1)}+(\sigma_0+s)^{-(k+1)}]$$
$$\times\log\hat{f}(s)ds=0, \tag{39}$$

where $\mathcal{C}_1$ is the line segment between $-jR$ and jR excluding $[j(\omega_\ell-\varepsilon),j(\omega_\ell+\varepsilon)]$; $\mathcal{C}_2$ is the right semicircle with radius R centered at the origin; $\mathcal{C}_3$ is the circle with radius ε centered at the σ_0; and $\mathcal{C}_4$ includes the right semicircles with radius ε centered at $j\omega_\ell$.

To show (28), we evaluate the integral paths in (39) for $k=0$, and let $R\to\infty$, $\varepsilon\to 0$. The result is

$$\int_{-\infty}^{\infty}[(\sigma_0-j\omega)^{-1}+(\sigma_0+j\omega)^{-1}]\log|f(j\omega)|d\omega$$
$$=2\pi\log|\hat{c}|.$$

We have $[(\sigma_0-j\omega)^{-1}+(\sigma_0+j\omega)^{-1}]\log|f(j\omega)|$ is an even function, and using (32) we get (28).

To show (29), we evaluate the integral paths in (39) for $k=1,2,\ldots,m-1$, and let $R\to\infty$, $\varepsilon\to 0$. The result is

$$\int_{-\infty}^{\infty}[(\sigma_0-j\omega)^{-(k+1)}+(\sigma_0+j\omega)^{-(k+1)}]\log|f(j\omega)|d\omega$$
$$=(-1)^k 2\pi\hat{a}_k.$$

We have $[(\sigma_0-j\omega)^{-(k+1)}+(\sigma_0+j\omega)^{-(k+1)}]\log|f(j\omega)|$ is an even function, and using (33) we get (29) for $k=1,2,\ldots,m-1$. This finishes the proof for $s_0=\sigma_0$.

4) $s_0 = \sigma_0 + j\omega_0$: For $s_0 = \sigma_0 + j\omega_0$, we show (28) and (29) by taking the contour integral of the following functions

$$[(s_0 - s)^{-(k+1)} + (s_0 + s)^{-(k+1)} + (s_0^* - s)^{-(k+1)} + (s_0^* + s)^{-(k+1)}] \log \hat{f}(s) \tag{40a}$$

$$[(s_0 - s)^{-(k+1)} + (s_0 + s)^{-(k+1)} - (s_0^* - s)^{-(k+1)} - (s_0^* + s)^{-(k+1)}] \log \hat{f}(s) \tag{40b}$$

along the close curve shown in Figure 9(d). These functions are analytic in the RHP except s_0 and s_0^*; they are also analytic on the imaginary axis except possible zeros and poles of $\hat{f}(s)$ on the imaginary axis, which we denote as $j\omega_\ell$. Therefore, the following contour integral is zero for $k = 0, 1, 2, \ldots, m-1$:

$$\int_{\mathcal{C}_1+\mathcal{C}_2+\mathcal{C}_3+\mathcal{C}_4} [(s_0 - s)^{-(k+1)} + (s_0 + s)^{-(k+1)} + (s_0^* - s)^{-(k+1)} + (s_0^* + s)^{-(k+1)}] \log \hat{f}(s) ds = 0, \tag{41a}$$

$$\int_{\mathcal{C}_1+\mathcal{C}_2+\mathcal{C}_3+\mathcal{C}_4} [(s_0 - s)^{-(k+1)} + (s_0 + s)^{-(k+1)} - (s_0^* - s)^{-(k+1)} - (s_0^* + s)^{-(k+1)}] \log \hat{f}(s) ds = 0, \tag{41b}$$

where $\mathcal{C}_1$ is the line segment between $-jR$ and jR excluding $[j(\omega_\ell - \varepsilon), j(\omega_\ell + \varepsilon)]$; $\mathcal{C}_2$ is the right semicircle with radius R centered at the origin; $\mathcal{C}_3$ includes the circles with radius ε centered at the s_0 and s_0^*; and $\mathcal{C}_4$ includes the right semicircles with radius ε centered at $j\omega_\ell$.

To show (28), we evaluate the integral paths in (41a) for $k = 0$, and let $R \to \infty$, $\varepsilon \to 0$. The result is

$$\int_{-\infty}^{\infty} \mathrm{Re}[(s_0 - j\omega)^{-1} + (s_0 + j\omega)^{-1}] \log |f(j\omega)| d\omega = 2\pi \log |\hat{c}|.$$

We have $\mathrm{Re}[(s_0 - j\omega)^{-1} + (s_0 + j\omega)^{-1}] \log |f(j\omega)|$ is an even function, and using (32) we get (28).

To show (29), we first evaluate the integral paths in (41) for $k = 1, 2, \ldots, m-1$, and let $R \to \infty$, $\varepsilon \to 0$. The result is

$$\int_{-\infty}^{\infty} [(s_0 - j\omega)^{-(k+1)} + (s_0 + j\omega)^{-(k+1)}] \log |f(j\omega)| d\omega = (-1)^k 2\pi \hat{a}_k.$$

We have $[(s_0 - j\omega)^{-(k+1)} + (s_0 + j\omega)^{-(k+1)}] \log |f(j\omega)|$ is an even function, and using (33) we get (29). This finishes the proof for $s_0 = \sigma_0 + j\omega_0$. ■

5) Remark on lemma 3: Because the formulas (28), (29) subtract or divide poles from zeros in equal quantity, when we apply Lemma 3 to $f(s) = \det A(s)$, (28), (29) still hold if the poles and zeros of the determinant are replaced by the poles and zeros of the matrix $A(s)$.

C. Preliminary lemmas on S-matrices

Lemma 4: If $\mathrm{Re}\{s_0\} > 0$ and the Darlington network given in Lemma 1 is used, then

$$\det S_{GM}(s_0) = \det S_{b22}(s_0) \neq 0, \tag{42}$$

and

$$\left(\sum_i (p_{GM,i} - s_0)^{-\ell} - \sum_i (z_{GM,i} - s_0)^{-\ell} \right) = \left(\sum_i (p_{b22,i} - s_0)^{-\ell} - \sum_i (z_{b22,i} - s_0)^{-\ell} \right) \tag{43}$$

for $\ell = 1, \ldots, m-1$.

If $\mathrm{Re}\{s_0\} = 0$, then m is even, (42) holds, and (43) holds for $\ell = 1, \ldots, m-2$.

If $\mathrm{Re}\{s_0\} = 0$ and $I - S_L(s_0)S_G(s_0)$ is non-singular then (43) holds for $\ell = m-1$.

If $\mathrm{Re}\{s_0\} = 0$ and $I - S_L(s_0)S_G(s_0)$ is singular then

$$(-1)^{\frac{m}{2}} \times \left(\sum_i (p_{GM,i} - s_0)^{-(m-1)} - \sum_i (z_{GM,i} - s_0)^{-(m-1)} \right) \leq (-1)^{\frac{m}{2}} \times \left(\sum_i (p_{b22,i} - s_0)^{-(m-1)} - \sum_i (z_{b22,i} - s_0)^{-(m-1)} \right). \tag{44}$$

Proof: We separate our discussion into two possibilities: $\mathrm{Re}\{s_0\} > 0$ and $\mathrm{Re}\{s_0\} = 0$.

1) Re$\{s_0\} > 0$: Because the Darlington network in Lemma 1 is assumed, $S_{b22}(s)$ has no zeros at $s = s_0$, for otherwise $S_L(s)$ would have zeros at $s = -s_0$, and therefore have poles at $s = s_0$ in order to satisfy (18). This contradicts $S_L(s)$ being Hurwitzian. Hence, $\det S_{b22}(s_0) \neq 0$, and $S_L(s)$ has no zeros at $s = -s_0$.

Since $S_b(s)$ is lossless and therefore $S_b^T(-s)S_b(s) = I$, we get $S_{b12}(s) = -S_L^{-T}(-s)S_{b21}^T(-s)S_{b22}(s)$. We manipulate (15) to get

$$S_{GM}(s) = [I - S_{b21}(s)S_G(s)(I - S_L(s)S_G(s))^{-1} \times S_L^{-T}(-s)S_{b21}^T(-s)]S_{b22}(s).$$

Taking determinant on both sides yields

$$\begin{aligned} \det S_{GM}(s) &= \det S_{b22}(s) \det[I - S_{b21}(s)S_G(s) \times (I - S_L(s)S_G(s))^{-1} S_L^{-T}(-s)S_{b21}^T(-s)] \\ &= \det S_{b22}(s) \det[I - S_{b21}^T(-s)S_{b21}(s)S_G(s) \times (I - S_L(s)S_G(s))^{-1} S_L^{-T}(-s)]. \end{aligned}$$

Since $S_L(s)$ and $S_G(s)$ are bounded, $S_L(s)S_G(s)$ is also bounded and $I - S_L(s_0)S_G(s_0)$ is non-singular for $\mathrm{Re}\{s_0\} > 0$ [24, 7.22]. Hence, $S_{b21}^T(-s)S_{b21}(s) = I - S_L^T(-s)S_L(s) = O((s - s_0)^m)$, and $S_L(-s_0)$ and $I - S_L(s_0)S_G(s_0)$ are non-singular. We then have

$$\det S_{GM}(s) = \det S_{b22}(s)[1 + O((s - s_0)^m)].$$

Thus $\det S_{b22}(s_0) = \det S_{GM}(s_0) \neq 0$, and (42) holds for $\mathrm{Re}\{s_0\} > 0$.

To show (43), we apply Lemma 2 to $\det S_{b22}(s)$ and $\det S_{GM}(s)$:

$$\begin{aligned} \log \det S_{GM}(s) &= a_0 + a_1(s - s_0) + \ldots + a_{m-1}(s - s_0)^{m-1} + \ldots \\ \log \det S_{b22}(s) &= b_0 + b_1(s - s_0) + \ldots + b_{m-1}(s - s_0)^{m-1} + \ldots, \end{aligned} \tag{45}$$

where a_ℓ and b_ℓ have the form (27). Because $\det S_{GM}(s) = \det S_{b22}(s) + O((s - s_0)^m)$, $a_\ell = b_\ell$ for $\ell = 0, 1, \ldots, m-1$. Writing a_ℓ and b_ℓ in the form of (27) yields (43).

2) Re$\{s_0\} = 0$: Let $s_0 = j\omega_0$. Since $S_b(s)$ is lossless and (18) is satisfied, $S_L^H(j\omega_0)S_L(j\omega_0) = S_{b22}^H(j\omega_0)S_{b22}(j\omega_0) = I$. Hence, $\det S_{b22}(j\omega_0) \neq 0$.

We begin by showing that m is even. We substitute $s = j(\omega_0 \pm \varepsilon)$ into (18):

$$\begin{aligned} &I - S_L^T(-j(\omega_0 \pm \varepsilon))S_L(j(\omega_0 \pm \varepsilon)) \\ &= I - S_L^H(j(\omega_0 \pm \varepsilon))S_L(j(\omega_0 \pm \varepsilon)) = A_m(\pm j\varepsilon)^m + \dots. \end{aligned}$$

Since $S_L(s)$ is bounded, the $A_m(\pm j\varepsilon)^m$ is positive semidefinite. With $A_m \neq 0$, it is possible only when m is even.

If $I - S_L(j\omega_0)S_G(j\omega_0)$ is non-singular, we follow a method similar to the Re$\{s_0\} > 0$ case to get $\det S_{GM}(s) = \det S_{b22}(s) + O((s - j\omega_0)^m)$. Thus (42) and (43) hold for $\ell = 1, 2, \dots, m-1$.

If $I - S_L(j\omega_0)S_G(j\omega_0)$ is singular, (44) can be proven in a manner similar to the proof of Lemma 5 in [9]. These steps are omitted. This finishes the proof of Lemma 4. ■

D. Proof of Theorem 2

We use the Darlington network in Lemma 1. Then Lemma 4 gives $\det S_{b22}(s_0) = \det S_{GM}(s_0) \neq 0$. Because $S_b(s)$ is para-unitary, (18) implies $\det(S_{b22}^T(-s)S_{b22}(s)) = \det(S_L^T(-s)S_L(s)) = 1 + O((s - s_0)^m)$. Hence, $\det S_{b22}(s)$ satisfies the conditions of Lemma 3.

From Lemma 4, $\det S_{GM}(s) = \det S_{b22}(s) + O((s - s_0)^m)$ for Re$\{s_0\} > 0$, and $\det S_{GM}(s) = \det S_{b22}(s) + O((s - s_0)^{m-1})$ for Re$\{s_0\} = 0$. When Re$\{s_0\} = 0$, we let $s_0 = j\omega_0$ and consider $s = j(\omega_0 \pm \varepsilon)$ for $\varepsilon > 0$:

$$\begin{aligned} &\det[S_{GM}^T(-j(\omega_0 \pm \varepsilon))S_{GM}(j(\omega_0 \pm \varepsilon))] \\ &= \det[S_{GM}^H(j(\omega_0 \pm \varepsilon))S_{GM}(j(\omega_0 \pm \varepsilon))] \\ &= 1 + b_{m-1}(\pm j\varepsilon)^{m-1} + O(\varepsilon^m) \leq 1. \end{aligned}$$

The inequality is because $S_{GM}(s)$ is bounded. Since $m-1$ is odd, $b_{m-1} = 0$. Hence, $\det(S_{GM}^T(-s)S_{GM}(s)) = 1 + O((s - s_0)^m)$, and $\det S_{GM}(s)$ satisfies the conditions of Lemma 3.

Unfortunately, Lemma 3 does not apply to $\det S_L(s)$ since there are possible zeros of $S_L(s)$ at $s = s_0$ when Re$\{s_0\} > 0$. From (18), if $S_L(s)$ has zeros at s_0, it also has zeros at s_0^* and poles at $-s_0, -s_0^*$; the multiplicities of these poles or zeros are equal. We therefore construct a function $\widehat{\det S_L}(s)$ by removing the poles at $-s_0, -s_0^*$ and zeros at s_0, s_0^* from $\det S_L(s)$, such that $|\widehat{\det S_L}(j\omega)| = |\det S_L(j\omega)|$. This function satisfies $\widehat{\det S_L}(-s)\widehat{\det S_L}(s) = 1 + O((s - s_0)^m)$ and $\widehat{\det S_L}(s_0) \neq 0$, thus the conditions of Lemma 3.

Since $S_b(s)$ is para-unitary, $|\det S_L(j\omega)| = |\det S_{b22}(j\omega)|$. It follows that

$$|\det S_L(j\omega)| = |\widehat{\det S_L}(j\omega)| = |\det S_{b22}(j\omega)|. \tag{46}$$

We first apply (28):

$$\begin{aligned} &\int_0^\infty \mathrm{Re}[(s_0 - j\omega)^{-1} + (s_0 + j\omega)^{-1}] \log|\det S_{GM}(j\omega)| d\omega \\ &= \pi \log\left|\det S_{GM}(s_0) \cdot \frac{\prod_i (s_0 + z_{GM+,i})}{\prod_i (s_0 - z_{GM+,i})}\right| \qquad (47a) \\ &\int_0^\infty \mathrm{Re}[(s_0 - j\omega)^{-1} + (s_0 + j\omega)^{-1}] \log|\det S_{b22}(j\omega)| d\omega \\ &= \pi \log\left|\det S_{b22}(s_0) \cdot \frac{\prod_i (s_0 + z_{b22+,i})}{\prod_i (s_0 - z_{b22+,i})}\right| \qquad (47b) \\ &\int_0^\infty \mathrm{Re}[(s_0 - j\omega)^{-1} + (s_0 + j\omega)^{-1}] \log|\widehat{\det S_L}(j\omega)| d\omega \\ &= \pi \log\left|\widehat{\det S_L}(s_0) \cdot \frac{\prod_i (s_0 + z_{L+,i})}{\prod_i (s_0 - z_{L+,i})}\right|. \qquad (47c) \end{aligned}$$

Note s_0 and s_0^* are excluded in $z_{L+,i}$ in (47c). From the definition of $\widehat{\det S_L}(s)$, we can rewrite (47c) as

$$\begin{aligned} &\int_0^\infty \mathrm{Re}[(s_0 - j\omega)^{-1} + (s_0 + j\omega)^{-1}] \log|\widehat{\det S_L}(j\omega)| d\omega \\ &= \pi \log\left|\det S_L(s_0) \cdot \frac{\prod_i (s_0 + z_{L+,i})}{\prod_i (s_0 - z_{L+,i})}\right|, \end{aligned} \tag{48}$$

with s_0 and s_0^* included in $z_{L+,i}$. Because of (46), the integral in (47b) is the same if we replace $|\det S_{b22}(j\omega)|$ with $|\widehat{\det S_L}(j\omega)|$. Hence, the right-hand sides of (47b) and (48) are equal. We now apply (42) in Lemma 4 to the right-hand sides of (47a) and (47b), and (17) in Lemma 1 to the right-hand side of (47b). The result is (20).

We then apply (29):

$$\begin{aligned} &\int_0^\infty [(s_0 - j\omega)^{-(k+1)} + (s_0 + j\omega)^{-(k+1)}] \\ &\times \log|\det S_{GM}(j\omega)| d\omega \\ &= \frac{(-1)^k \pi}{k}\Big[\sum_i (p_{GM,i} - s_0)^{-k} - \sum_i (z_{GM,i} - s_0)^{-k} \\ &+ \Big(\sum_i (z_{GM+,i} - s_0)^{-k} - \sum_i (-z_{GM+,i} - s_0)^{-k}\Big)\Big] \end{aligned} \tag{49a}$$

$$\begin{aligned} &\int_0^\infty [(s_0 - j\omega)^{-(k+1)} + (s_0 + j\omega)^{-(k+1)}] \\ &\times \log|\det S_{b22}(j\omega)| d\omega \\ &= \frac{(-1)^k \pi}{k}\Big[\sum_i (p_{b22,i} - s_0)^{-k} - \sum_i (z_{b22,i} - s_0)^{-k} \\ &+ \Big(\sum_i (z_{b22+,i} - s_0)^{-k} - \sum_i (-z_{b22+,i} - s_0)^{-k}\Big)\Big] \end{aligned} \tag{49b}$$

$$\begin{aligned} &\int_0^\infty [(s_0 - j\omega)^{-(k+1)} + (s_0 + j\omega)^{-(k+1)}] \\ &\times \log|\widehat{\det S_L}(j\omega)| d\omega \\ &= \frac{(-1)^k \pi}{k}\Big[\sum_i (p_{L,i} - s_0)^{-k} - \sum_i (z_{L,i} - s_0)^{-k} \\ &+ \Big(\sum_i (z_{L+,i} - s_0)^{-k} - \sum_i (-z_{L+,i} - s_0)^{-k}\Big)\Big], \end{aligned} \tag{49c}$$

where $k = 1, 2, \dots, m-1$. Note $-s_0$ and $-s_0^*$ are excluded in $p_{L,i}$, and s_0 and s_0^* are excluded in $z_{L,i}$ and $z_{L+,i}$ in (49c). Because of (46), the integral in (49b) is the same if we replace $|\det S_{b22}(j\omega)|$ with $|\widehat{\det S_L}(j\omega)|$. Hence, the right-hand sides of (49b) and (49c) are equal.

When $k \neq m-1$ or $I - S_L(s_0)S_G(s_0)$ is non-singular, we apply (43) in Lemma 4 to the right-hand sides of (49a) and (49b), and (17) in Lemma 1 to the right-hand side of (49b). The result is (21).

When $k = m - 1$ and $I - S_L(s_0)S_G(s_0)$ is singular, we apply (44) instead of (43) to the right-hand sides of (49a) and (49b). The result is (22). ■

REFERENCES

[1] D. Nie and B. M. Hochwald, "Bandwidth analysis of multiport radio-frequency systems—Part I," submitted to *IEEE Trans. Ant. Prop.*, Oct. 2015.

[2] H. W. Bode, *Network Analysis and Feedback Amplifier Design,* New York, NY, USA: Van Nostrand, 1945.

[3] R. M. Fano, "Theoretical limitations on the broadband matching of arbitrary impedances," *Journal of the Franklin Institute,* 249(1) pp. 57–83, and 249(2), pp. 139–154, 1950.

[4] B. Gustavsen and A. Semlyen, "Rational approximation of frequency domain responses by vector fitting," *IEEE Trans. Power Del.,* vol. 14, no. 3, pp. 1052–1061, July 1999.

[5] B. Gustavsen, "Improving the pole relocating properties of vector fitting," *IEEE Trans. Power Del.,* vol. 21, no. 3, pp. 1587–1592, July 2006.

[6] D. Deschrijver, M. Mrozowski, T. Dhaene and D. De Zutter, "Macromodeling of multiport systems using a fast implementation of the vector fitting method," *IEEE Micro. Wireless Comp. Let.,* vol. 18, no. 6, pp. 383–385, June 2008.

[7] B. Gustavsen and A. Semlyen, "Fast passivity assessment for S-parameter rational models via a half-size test matrix," *IEEE Trans. Micro. Thy. Tech.,* vol. 56, no. 12, pp. 2701–2708, Dec. 2008.

[8] B. Gustavsen, "Fast passivity enforcement for S-parameter models by perturbation of residue matrix eigenvalues," *IEEE Trans. Adv. Pack.,* vol. 33, no. 1, pp. 257–265, Feb. 2010.

[9] D. Nie and B. M. Hochwald, "Broadband matching bounds for coupled loads," *IEEE Trans. Circ. Sys. I: Regular Papers,* vol. 62, no. 4, pp. 995–1004, April 2015.

[10] P. I. Richards, "Resistor-transmission-line circuits," *Proc. IRE*, vol. 36, no. 2, pp. 217–220, 1948.

[11] L. Besser and R. Gilmore, *Practical RF circuit design for modern wireless systems, vol. 1: Passive circuits and systems* Norwood, MA: Artech House, 2003.

[12] J. J. Adams and J. T. Bernhard, "Broadband equivalent circuit models for antenna impedances and fields using characteristic modes," *IEEE Trans. Ant. Prop.*, vol. 61, no. 8, pp. 3985–3994, Aug. 2013.

[13] J. Helton and O. Merino, *Classical Control Using H^∞ Methods*, Society for Industrial and Applied Mathematics, 1998.

[14] E. M. Stein and R. Shakarchi, *Complex Analysis, Vol. 2,* Princeton, NJ: Princeton University Press, 2010.

[15] G. H. Golub and C. F. Van Loan, *Matrix Computations,* 4th ed., Baltimore, MD: JHU Press, 2012.

[16] S. Skogestad and I. Postlethwaite, *Multivariable Feedback Control: Analysis and Design,* 2nd ed., Hoboken, NJ: Wiley, 2005.

[17] J. Helton, P. Spain, and N. Young, "Tracking poles and representing Hankel operators directly from data," Numer. Math. vol. 58, pp. 641–660, 1991.

[18] J. Helton, P. Spain, and N. Young, "Tracking poles, representing Hankel operators, and the Nehari problem," Linear Algebra and its Applications, vol. 223, pp. 637–694, 1995.

[19] H. J. Carlin, "A new approach to gain-bandwidth problems," *IEEE Trans. Circ. Sys.*, vol. 24, no. 4, pp. 170–175, April 1977.

[20] S. Darlington, "Synthesis of reactance 4-poles," *Journal of Mathematics and Physics,* vol. XVIII, pp. 275–353, Sep. 1939.

[21] D. Nie, B. M. Hochwald and E. Stauffer, "Systematic design of large-scale multiport decoupling networks," *IEEE Trans. Circ. Sys. I: Regular Papers,* vol. 61, no. 7, pp. 2172–2181, July 2014.

[22] R. W. Newcomb, "On the n-port Brune resistance extraction," *IEEE Trans. Circ. Thy.,* vol. 10, no. 1, pp. 125–125, March 1963.

[23] R. W. Newcomb, *Linear Multiport Synthesis,* New York, NY: McGraw-Hill Book Company, 1966.

[24] V. Belevitch, *Classical Network Theory,* San Francisco, CA: Holden-Day, 1968.

[25] M. R. Wohlers, *Lumped and Distributed Passive Networks: A Generalized and Advanced Viewpoint,* New York, NY: Academic Press, 1969.

[26] R. Douglas, J. Helton, "The precise theoretical limits of causal Darlington synthesis," *IEEE Trans. Circ. Thy.,* vol. 20, no. 3, pp. 327–327, May 1973.

[27] C. J. Galbraith, R. D. White, L. Cheng, K. Grosh and G. M. Rebeiz, "Cochlea-based RF channelizing filters," *IEEE Trans. Circ. Sys. I: Regular Papers,* vol. 55, no. 4, pp. 969–979, May 2008.

[28] L. J. Chu, "Physical limitations of omni-directional antennas," *J. Appl. Phys.,* vol. 19, no. 12, pp. 1163–1175, Dec. 1948.

[29] M. Gustafsson, C. Sohl and G. Kristensson, "Physical limitations on antennas of arbitrary shape," *Proc. R. Soc. A,* vol. 463, pp. 2589–2607, Oct. 2007.

[30] C. Sohl and M. Gustafsson, "A priori estimates on the partial realized gain of ultra-wideband (UWB) antennas," *Quart. J. Mech. Appl. Math.,* vol. 61, no. 3, pp. 415–430, 2008.

[31] M. Gustafsson, C. Sohl and G. Kristensson, "Illustrations of new physical bounds on linearly polarized antennas," *IEEE Trans. Ant. Prop.*, vol. 57, no. 5, pp. 1319–1327, May 2009.

[32] E. Telatar, "Capacity of multi-antenna Gaussian channels," *Eur. Trans. Telecomm.*, vol. 10, pp. 585–595, 1999.